



**HAL**  
open science

# Antibacterial and Biofilm-Preventive Photocatalytic Activity and Mechanisms on P/F-Modified TiO<sub>2</sub> Coatings

Yige Yan, Charline Soraru, Valérie Keller, Nicolas Keller, Lydie Ploux

► **To cite this version:**

Yige Yan, Charline Soraru, Valérie Keller, Nicolas Keller, Lydie Ploux. Antibacterial and Biofilm-Preventive Photocatalytic Activity and Mechanisms on P/F-Modified TiO<sub>2</sub> Coatings. ACS Applied Bio Materials, 2020, 3 (9), pp.5687-5698. 10.1021/acsabm.0c00467 . hal-03031805

**HAL Id: hal-03031805**

**<https://hal.science/hal-03031805>**

Submitted on 30 Nov 2020

**HAL** is a multi-disciplinary open access archive for the deposit and dissemination of scientific research documents, whether they are published or not. The documents may come from teaching and research institutions in France or abroad, or from public or private research centers.

L'archive ouverte pluridisciplinaire **HAL**, est destinée au dépôt et à la diffusion de documents scientifiques de niveau recherche, publiés ou non, émanant des établissements d'enseignement et de recherche français ou étrangers, des laboratoires publics ou privés.

---

# Antibacterial and biofilm-preventive photocatalytic activity and mechanisms on P/F-modified TiO<sub>2</sub> coatings

*Yige Yan<sup>b,c</sup>, Charline Soraru<sup>c</sup>, Valérie Keller<sup>b</sup>, Nicolas Keller<sup>b</sup>, Lydie Ploux<sup>a,c\*</sup>*

<sup>a</sup> *BioMaterials and BioEngineering, U1121, INSERM / Université de Strasbourg-Faculté Dentaire, 11 rue Humann, 67000 Strasbourg, France*

<sup>b</sup> *Institut de Chimie et Procédés pour l'Energie, l'Environnement et la Santé (ICPEES), UMR7515, CNRS / Université de Strasbourg, 25 rue Becquerel, 67087 Strasbourg Cedex, France*

<sup>c</sup> *Institut de Science des Matériaux de Mulhouse (IS2M), UMR7361, CNRS / Université de Haute Alsace, 15 rue Jean Starcky, 68057 Mulhouse cedex, France*

---

## KEYWORDS:

Antibacterial P/F-modified TiO<sub>2</sub> coating, photocatalytic activity, immediate versus long-term biofilm-preventive activity, mechanism, surface topographic properties.

## ABSTRACT

Photocatalytic antibacterial and biofilm-preventive activity in liquid of heavy-metal-free coatings based on a phosphorus (P) and fluorine (F) -modified TiO<sub>2</sub> photocatalyst has been investigated. They reveal significantly higher immediate and longer-term (biofilm-preventive) inactivation capacity than a reference coating made of the commercial photocatalyst TiO<sub>2</sub> P25 on three bacterial species differing in cell wall type and ability to resist oxidative stress (*Escherichia coli*, *Staphylococcus epidermidis*, *Pseudomonas fluorescens*) (up to more than 99% reduction of colonization on P/F-modified TiO<sub>2</sub> coating compared to about 50% on P25 TiO<sub>2</sub> coating for 10 min UV-A illumination). This results from the P- and F-induced improvement of photocatalyst properties and from the smoother surface topography, which shortens reactive oxygen species (ROSs) diffusion to the outer membrane of the targeted adhered bacteria. Decrease in ROSs-related impairment of cell wall, respiratory and enzymatic activities confirms the loss of ROSs throughout the bacterial cell degradation. *Staphylococcus epidermidis* and *Pseudomonas fluorescens* are less sensitive than *Escherichia coli*, with a probable relation to the bacterial oxygen stress defense mechanism. The coating antibacterial efficacy was highly affected by phosphate ions and the richness in dissolved oxygen of the reaction medium.

---

## 1. Introduction

Surface adhesion of bacteria and formation of biofilm<sup>1</sup> present health threat in many instances such as biomedical field,<sup>2</sup> food industry,<sup>3</sup> water distribution<sup>4</sup> and wastewater treatment.<sup>5</sup> Apart from conventional physico-chemical surface treatments, an alternative method for reducing frequency and level of surface contamination has been proposed in the last two decades: the self-disinfecting surfaces.<sup>6-8</sup> Nowadays, surfaces impregnated, functionalized or coated with silver or copper are the most advanced.<sup>9</sup> However, the development of surfaces with active biocidal agent but harmless doses for human health is delicate.<sup>10</sup> As a consequence of the surface redox properties developed by the TiO<sub>2</sub> semiconductor under ultraviolet A irradiation (UVA, 320–400 nm), TiO<sub>2</sub> mostly in its anatase form exhibits strong antibacterial effect owing to the generation of various reactive oxygen species (ROSs) from photogenerated charges.<sup>11</sup> Applying TiO<sub>2</sub>-incorporated surfaces for self-disinfection enabled bacterial inactivation, even up to complete mineralization<sup>12-13</sup> on a wide range of Gram-negative and Gram-positive bacteria species.

Aside from irradiation source power,<sup>14</sup> treatment time<sup>15</sup> and matrix (or substrate)-related factors,<sup>16-17</sup> the intrinsic physico-chemical properties of TiO<sub>2</sub> greatly affect the photocatalytic oxidation performance of the coating by influencing the amount, recombination rate and diffusion length of the photogenerated charges.<sup>18</sup> The role of TiO<sub>2</sub> itself was addressed in many studies by comparing the bactericidal performance of new TiO<sub>2</sub> coatings<sup>19</sup> to that made of P25 TiO<sub>2</sub>,<sup>20</sup> the commercial photocatalyst largely admitted as a reference. The self-disinfection properties were improved thanks to chemical modifications of TiO<sub>2</sub>, mainly involving Ag and Cu. However, Ag/Cu-modified TiO<sub>2</sub> is expected to reveal high bactericidal properties directly due to the heavy metals.<sup>21</sup> Other studies focused on the building of TiO<sub>2</sub>-based heterojunctions<sup>22</sup> or TiO<sub>2</sub> doping,<sup>23</sup> to provide self-

---

disinfection properties under visible light. Meanwhile, TiO<sub>2</sub> coatings with extended bactericidal efficiency under UVA irradiation without releasing of environmental-unfriendly agents such as heavy metals are lacking.

Efficacy of TiO<sub>2</sub>-based self-disinfection coatings also depends on the surface-related properties, especially those resulting from the weight of TiO<sub>2</sub> deposited per surface area as well as from the surface morphology and texture, closely related to the size of the particles or of their aggregates. They directly impact the photocatalytic activity<sup>16</sup> and also change the surface area of contact between TiO<sub>2</sub> and the adhered bacteria, thus affecting the degree of ROSs attack on cells. Further, both chemical and topographical surface properties, which change with the photocatalyst density and chemistry, modulate the amount of adhered and hence targeted bacteria.<sup>24</sup> If present, the matrix in which the particles are embedded also modulates the disinfection efficiency by influencing bacterial adhesion<sup>25-26</sup> and may create a synergetic effect with the photocatalyst.<sup>18</sup> Other factors like the presence of ions and the oxygen content in the liquid environment may also influence the photocatalytic activity, thus having dramatic consequences for the performance in real aqueous phase conditions.<sup>27</sup> However, except regarding the matrix, these topics are usually omitted.

Besides, bacterial inactivation on TiO<sub>2</sub>-based coatings is usually addressed by counting viable or cell wall-damaged cells.<sup>11</sup> Rare studies also investigate the photocatalytic toxicity to intracellular functions such as enzymatic and respiratory activities.<sup>28-29</sup> However, they only touch upon TiO<sub>2</sub> nanoparticles or nanocomposites but fail for TiO<sub>2</sub> coatings. Hence, actual impairment of vital intracellular functions in bacteria adhered and treated thanks to TiO<sub>2</sub> coatings has still to be clarified. Besides, bacteria are able to overcome the photocatalytic treatment thanks to ROSs defense mechanisms involving catalase and superoxide dismutase (SOD).<sup>30-31</sup> In the case of

---

oxidative damages caused by TiO<sub>2</sub>, the immediate inactivation rate of bacteria was shown to be inversely proportional to SOD and catalase activities.<sup>32</sup> In addition, a SOD- and catalase-deficient mutant strain was reported to be much more sensitive to photocatalytic treatment than the wild strain.<sup>33</sup> Importantly, this capacity varies with species and strains<sup>30</sup> and can enable bacterial repair during the post-irradiation period.<sup>34</sup> Accordingly, the high immediate antibacterial efficacy of a self-disinfection coating cannot ensure high post-photocatalytic longer-term performance. To our knowledge, this has been never investigated for immobilized TiO<sub>2</sub> especially regarding variations according to bacterial species and their sensitivity to oxidative stress.

We report here the photocatalytic liquid-phase antibacterial activity of a novel phosphorus (P) and fluorine (F) -modified TiO<sub>2</sub> photocatalyst immobilized as a coating, which is expected to provide higher bactericidal efficiency under UVA light than a reference coating made of TiO<sub>2</sub> P25 catalyst without releasing any environmental-unfriendly agent. The P/F-modified TiO<sub>2</sub> powder was developed in a previous work and revealed higher activity in the photocatalytic degradation of gaseous methylethylketone compared to TiO<sub>2</sub> P25.<sup>35</sup> Here, both immediate curative performance and the corresponding longer-term biofilm-preventive antibacterial efficacy of the TiO<sub>2</sub> coatings were analyzed, for the first time, by *in situ* monitoring growth of bacteria adhered on such coatings. Impact of the photocatalytic treatment on the cell wall and on the vital respiratory and enzymatic functions was also *in situ* studied by following cell wall permeability as well as redox and esterase activities. Potential effect of the cell wall type and ability to resist oxidative stress of bacteria was questioned by using three bacterial species (*E. coli*, *Staphylococcus epidermidis* (*S. epidermidis*) and *Pseudomonas fluorescens* (*P. fluorescens*)) differing in these terms. Possible correlations between physical surface characteristics of the coating and chemical intrinsic properties of the

---

TiO<sub>2</sub> photocatalyst on one side, and the antibacterial efficacy on the other side were considered. Effects of certain ions and richness in dissolved oxygen of the reaction medium were also explored.

## 2. Experimental

### 2.1. Sample preparation

Aeroxide® P25 TiO<sub>2</sub> photocatalyst was purchased from Evonik® (Evonik Resource Efficiency GmbH, Hanau-Wolfgang, Germany) and is referred to as “P25”.

The synthesis of the novel P/F-modified TiO<sub>2</sub> photocatalyst was described elsewhere.<sup>35</sup> Briefly, 5 g of titanium (IV) isopropoxide (Ti(O<sup>i</sup>Pr)<sub>4</sub>, 97%, Aldrich) was mixed in 10 g of propan-2-ol (AnalaR Normapur, >99.5%, VWR Chemicals), before 6.2 g of 2.2 mol/L acetic acid solution containing 21.7 mg of sodium fluoride (NaF, ACS reagent, ≥99%, Sigma-Aldrich) and 59 mg of phosphoric acid (H<sub>3</sub>PO<sub>4</sub> (PA), analytical reagent, ≥85%, R.P.Normapur) was further added dropwise. NaF and PA additives provided the fluoride anions (F<sup>-</sup>) and the phosphate anions to the synthesis medium, respectively, with a F/Ti and P/Ti molar ratio of 0.03. A white milky precipitate was formed immediately, and the solution was kept under stirring for 1 h before being further sealed by parafilm and aged at room temperature for 6 days without any stirring to partially generate anatase nanoparticles by crystallization. After filtration of the powder from the rest of the solvent, the solid was dispersed in 50 mL distilled water under stirring for 10 min, before being separated from liquid by centrifuge. The washing-centrifuge cycle was repeated 2 times. After drying for 2 h at 100 °C, the so-obtained white powder was finally calcined in air at 550°C for 2 h with a heating rate of 5°C/min in attempt to increase crystallinity and to remove fluorine adsorbed on the sample surface.<sup>36</sup> This sample is referred to as “PANaF”.

---

For the preparation of coatings, 484 mg of both TiO<sub>2</sub> photocatalysts were separately dispersed in 1 ml of 96% ethanol (0.484 g/ml) followed by 5 min of ultrasonication in a 100 W ultrasonic cleaner. Then the TiO<sub>2</sub> suspensions were evenly deposited on borosilicate glass cover slips (ROTH Karlsruhe Deckglaser 22 x 22 mm) by drop casting with a surface density of 1 mg/cm<sup>2</sup>, while the substrates were continuously dried from below with a hairdryer. Drying was completed in several minutes. Both TiO<sub>2</sub> immobilized samples are referred to as “TiO<sub>2</sub> coatings”.

## **2.2. Characterization of photocatalysts**

X-ray diffraction (XRD) patterns of TiO<sub>2</sub> powders were recorded on a D8 Advance Bruker powder diffractometer in a  $\theta/\theta$  mode and using the K $\alpha_1$  radiation of Cu at 1.5406 Å. Surface area of TiO<sub>2</sub> powders were measured on an ASAP2010 Micromeritics Tristar 3000 analyzer using N<sub>2</sub> as an adsorbent at 77K. Before N<sub>2</sub> adsorption, samples were outgassed at 150°C for 12 h. BET surface area was calculated from the N<sub>2</sub> adsorption isotherm.

Transmission Electron Microscopy (TEM) analysis of TiO<sub>2</sub> powders was performed using a Philips CM200 in standard mode observation, equipped with thermo-ionic LaB<sub>6</sub> filament, operating at a 200 kV acceleration voltage. Samples were firstly grinded and sonicated in ethanol solution, before a drop of the solution was deposited onto a copper grid covered by holey carbon membrane for observation.

Surface topographical properties of TiO<sub>2</sub> coatings were analyzed by AFM by using a NanoScope IIIa with the following parameter settings: Tapping mode; Tip thickness of 7  $\mu$ l, length of 225  $\mu$ m, width of 38  $\mu$ m; Resonance frequency of 190 KHz; Force constant of 13-77 N/m; Image size of

---

1 $\mu$ m x 1 $\mu$ m for 5 different zones on each sample. Surface roughness was extracted from each micrograph after adequate image treatment and analysis by WSxM 9.1 ([www.wsxm.es](http://www.wsxm.es)).

X-ray Photoelectron Spectroscopy (XPS) surface characterization was performed on an XPS spectrometer SES-2002 (VG SCIENTA) apparatus equipped with an Al K $\alpha$  (1448.6 eV) source with a pass energy of 20 eV. The spectra were decomposed assuming contributions with Doniac-Sunjic shape<sup>37</sup> and Shirley background subtraction.<sup>38</sup>

### 2.3. Bacteria strains and culture methods

-80°C frozen bacterial cells were spread on LB (Lysogeny broth, Sigma-Aldrich) agar plate and cultured for two nights at 30°C for *E. coli* SCC1,<sup>39</sup> or 37°C for *S. epidermidis* ATCC 35983 (CIP 106510), or on BHI (Brain-Heart-Infusion, Sigma-Aldrich) agar plate at 30°C for *P. fluorescens* ATCC 13525 (CIP 69.13T). Then, precultures were prepared with one colony of *E. coli* or *S. epidermidis* in LB, or of *P. fluorescens* in BHI, before overnight incubation at 30°C, 37°C and 30°C, respectively. Cultures were prepared with 10% volume of the precultures in fresh LB for *E. coli* and *S. epidermidis*, and with 33.3% volume of the preculture in fresh BHI for *P. fluorescens*. Cultures were then incubated for 4 h at 30°C or 37°C before bacteria were harvested by centrifugation. Harvested bacteria pellets were re-suspended either in physiological NaCl (9 g/L, pH 6.8) solution or in the so-called M63G, a *E. coli*-selective minimum medium (pH 6.8).<sup>40</sup> The obtained bacterial suspensions were adjusted to an absorbance at 600 nm ( $A_{600\text{ nm}}$ ) of 0.1 ( $5 \times 10^7$  CFU mL<sup>-1</sup>) for being ready to inoculate the TiO<sub>2</sub> coatings. As a reference, i.e. internal control of bacterial adhesion and sessile population growth, cleaned borosilicate glass cover slip surface was inoculated and further analyzed similarly to the TiO<sub>2</sub> coatings.

---

## 2.4. Photocatalytic antibacterial activity of TiO<sub>2</sub> coatings

### 2.4.1. Immediate antibacterial effect

Coatings were sterilized by UVC irradiation ( $\lambda=245$  nm) for 7 min at a 2 cm distance before immersion in 3 ml of freshly-prepared M63G medium (exclusively for *E. coli*) or physiological NaCl (9 g/L) medium (for all three species) in Petri dishes (ROTH, standard petri dish, PS, 35 mm diameter, 10 mm height). After 3 h of incubation at 30°C or 37°C, the coatings were washed three times by 2 ml physiological NaCl without creating air-surface interface and ended being immersed in the last washing solution. Two of the three identical coatings of each type were exposed for 10 min or 45 min (and 3 h if necessary *i.e.* only for *P. fluorescens*) to UVA irradiation. The third coating was maintained without irradiation as a non-illuminated reference. The UVA irradiation was provided by using a 8W UV-A blacklight lamp (Sylvania Blacklight Blue F8W/BLB T5) located at a 1.5 cm distance above the coating samples (light distribution centered on  $\lambda=365$  nm with a received irradiance of 30 W/m<sup>2</sup> recorded using a RPS900-W ILT wideband spectroradiometer). For each illumination duration on control, P25 and PANaF coatings, experiments were repeated three times using three identical coating duplicates of each coating type. A last washing was performed after photocatalytic treatment to remove any planktonic bacteria. And in this last washing solution, Fluorescent Syto9® (Aldrich-Sigma) and propidium iodide (PI, Aldrich-Sigma) dyes were added (no Syto9® stain for *E. coli* SCC1) to stain viable or membrane-damaged bacteria respectively.

Observations of coating's colonization by bacteria were then conducted under confocal microscope (LSM700, Carl ZEISS) equipped with a X63 water immersion objective (W Plan

---

Apochromat X63/1.0, 2.0 mm) and working in fluorescence mode with the excitation laser at 488 nm and with acquisition wavelength at 528 nm and 645 nm for Syto9® (GFP for *E. coli* SCC1) and PI emission, respectively. Bacteria with active green GFP metabolism (for *E. coli*) or stained in green by Syto9® (for *S. epidermidis* and *P. fluorescens*) are called “Live” in the following text, while those with damaged membrane as demonstrated by the red staining of PI (for all bacteria species), are called “Damaged” in the following text. The obtained double-channel images in RGB form were analyzed *via* ImageJ 1.47V® software to access quantity of stained bacteria in terms of surface coverage fraction. Three different locations of each surface sample were observed, located on the diagonal line (Figure S1).

#### 2.4.2. Longer-term biofilm-preventive antibacterial effect

The longer-term antibacterial efficiencies of the coatings, *i.e.* post photocatalytic action, were determined for different UVA illumination durations. The general procedure is similar to that conducted for immediate antibacterial effect analysis, except that the coatings were put back into an adequate nutritive culture medium immediately after UVA illumination. They were kept overnight at 30°C or 37°C for *E. coli* or *P. fluorescens*, and *S. epidermidis* respectively, before being washed and stained for the final confocal microscopy observation. For the *P. fluorescens* strain, a 3 h UVA illumination experiment was also performed.

#### 2.4.3. Photocatalytic action mechanism

The experimental procedure was similar to that used for the analysis of immediate antibacterial photocatalytic effect but conducted on *E. coli* PHL 628, a biofilm-making K12 MG1655 derivative strain<sup>41</sup> without fluorescence properties like that of *E. coli* SCC1. After UVA illumination, Calcein AM (CAM, Aldrich-Sigma) and 5-cyano-2,3-ditolyl tetrazolium chloride (CTC, Aldrich-Sigma) fluorescent dyes were simultaneously used to stain bacteria with intact endogenous intracellular

---

esterase activities and redox respiratory activities respectively. Staining was performed in LB medium to reach a detectable level of bacterial respiratory activity.<sup>42</sup> On each surface sample, NaCl 9 g/L solution was thus replaced by 2 ml of solutions of CAM (3 mmol/L) and CTC (1 mmol/L) dyes in LB before 20 min incubation. Surface samples were then washed once by physiological NaCl 9 g/L medium without creating air-surface interface and finally observed under confocal microscope as described above. Excitation laser was at 488 nm and the emission was observed at 520 nm for CAM and 630 nm for CTC.

#### 2.4.4. Photocatalytic bactericidal action in oxygen-deficient condition

Immediate antibacterial effect of photocatalysis in oxygen-deficient condition has been evaluated on the *E. coli* SCC1 strain cultured in a confined environment (Figure S2). Briefly, 20  $\mu$ l of bacterial suspension prepared with freshly-autoclaved medium (therefore with oxygen deficiency) was dropped on each coating, which was immediately covered by a glass cover slip. The air-liquid exchange interface area was thus limited at the outer edge of the double glass cover layer. Then UVA illumination was performed as described above and prolonged up to 3 h since the photocatalytic activity was expected to drastically decrease in confined environment. In addition to the confocal microscopy analysis performed as described above, quantity of sessile bacteria was also assessed by using a classical plate counting method.<sup>43</sup> Glass cover slip was confirmed not to absorb neither UVA nor the fluorescence emitted by bacteria or bacterial staining.

Besides, the variation of the oxygen content during the photocatalysis action in confined environment was monitored by using an oxygen sensor patch (HIOXY Oxygen Sensor patch, IDIL). In the above described confined environment setup, the patch was stuck on the interior side of the top cover slip, sandwiching liquid along with the TiO<sub>2</sub> coating (Figure S3). The liquid used in this experiment was either distilled water, fresh bacteria-free physiological NaCl 9 g/L medium

---

or bacteria suspension adjusted to an absorbance  $A_{600\text{ nm}}$  of 0.1 or 1.0. Oxygen dissolved in liquid quenches the fluorescence of the sensor, allowing a modulation of the fluorescence intensity level *vs.* the dissolved oxygen concentration by observation under an up-right epifluorescence microscope (Olympus BX51). Excitation laser was at 405 nm and emission was observed at 630 nm. UVA illumination was applied on the bottom side of the coatings with the same irradiance as before. To compare the oxygen content with and without UVA illumination, micrographs were taken with both non-illuminated and illuminated coatings.

#### 2.4.5. Data statistics

Significance of the two-by-two differences between averages of bacteria's quantity on the diverse coatings was evaluated by bilateral Student's *t* tests with significance thresholds of 0.05. According to Scherrer,<sup>44</sup> the alternative hypothesis ( $H_1: \mu_{P25} \neq \mu_{PANAf}$ ) was assumed to be true when the main hypothesis ( $H_0: \mu_{P25} = \mu_{PANAf}$ ) was rejected.

### 3. Results and discussion

#### 3.1. Immediate photocatalytic antibacterial effect on *E. coli* SCC1

Surface fraction covered by *E. coli* SCC1 before and after illumination on the reference surface, P/F-modified and P25 TiO<sub>2</sub> coatings are shown in Figure 1 and Figure S4. Colonization was similar before illumination on all the three types of surface (TiO<sub>2</sub> coatings and reference), which indicates that the TiO<sub>2</sub> coatings do not present any noticeable attractive or repellent properties for bacteria compared to the reference. After surface inoculation and subsequent bacterial adhesion, no significant bacterial growth was observed neither on the reference surface nor on the TiO<sub>2</sub> coatings, as expected in NaCl 9 g/L medium. Regarding immediate photocatalytic effect, a 10 min

---

UVA treatment resulted in a strong reduction of bacterial activity on P/F-modified TiO<sub>2</sub> (“PANaF”) coating, with almost complete elimination of the sessile “Live” population. In contrast, a 10 min UVA treatment on P25 coating only provided about 50% of “Live” population decrease, with high variability of the results with samples and locations on samples. This is illustrated by the confocal micrographs in Figure S5 B, C, which display very different ratios of “Live” to “Damaged” bacteria numbers depending on the analyzed region on P25 coatings. After 45 min of UVA illumination however, a similar strong reduction of the quantity of “Live” bacteria was observed on PANaF and P25 coatings. Besides, the quantity of “Damaged” bacteria increased with the irradiation time up to the colonization level by “Live” bacteria measured before illumination. The average “Damaged” gain-to-“Live” loss ratios for 10 min and 45 min illumination are 1.71 and 0.84 on P25 coatings, and 1.09 and 1.15 on PANaF coating respectively. In general, good correlation was found between loss in “Live” bacteria and gain in “Damaged” bacteria for all the coatings and all illumination time. This clearly indicates that bacteria were not eradicated; rather their cell wall was more or less strongly degraded according to coating type and illumination time.

Immediately after 10 min of UVA illumination, enzymatic and respiratory activities of bacteria on TiO<sub>2</sub> coatings were not affected (Figure 2, Figure S6, Figure S7 and Figure S8), as shown by the absence of any significant difference in the quantities of CAM- or CTC-positive bacteria respectively. In contrast, 45 min illumination resulted in a strong reduction in the quantity of CTC-positive bacteria on both coating types, which was more significant on the PANaF coating. Reduction in respiratory activity is in accordance with the increase in physical damage of the cell wall, as shown by PI staining. A 45 min photocatalytic treatment also resulted in a loss in the quantity of CAM-positive bacteria, which was also more marked on PANaF coating than on P25 coating. This is indicative that bacteria have been hit at a sufficient level to inhibit any enzymatic

---

activity in a large part of the bacterial population (80% and 60% on PANaF and P25 coatings, respectively), even though cells were not completely degraded.

### **3.2. Relation between the physico-chemical properties of the coating and the antibacterial activity on *E. coli* SCC1**

PANaF TiO<sub>2</sub> coatings present higher photocatalytic activity than the P25 reference coating in terms of immediate cell wall damage and reduction in vital metabolic activities of *E. coli* cell. Experiments conducted without illumination or without TiO<sub>2</sub> coatings demonstrated that neither UVA illumination nor TiO<sub>2</sub> coatings were able by themselves to induce these antibacterial effects. Absence of toxicity of TiO<sub>2</sub> coatings was made sure by the preservation of very high “Live” and very low “Damaged” bacteria’s quantity on TiO<sub>2</sub> coating samples in the absence of illumination (Figure S4, Figure S9). In addition, neither 10 min (data not shown) nor 45 min of UVA illumination (Figure S9) resulted in any loss of “Live” bacteria and any gain of “Damaged” ones on reference surfaces. The applied irradiance was thus unable to induce any detectable damage of bacterial cells. 3 h of UVA illumination had to be reached to achieve a slight killing effect on *E. coli* SCC1, with non-significant variation of the “Live” bacteria population but high increase in the “Damaged” population (Figure S10). In addition, the electrostatic interactions between the charged bacterial outer surface (negative for all known bacterial species at physiological pH, about 7) and the material surface, which are known to impact bacterial adhesion,<sup>1</sup> are expected to have been similar on TiO<sub>2</sub> P25 and PANaF materials.<sup>45</sup> Both materials exhibit isoelectric point (IEP) of  $5.6 \pm 0.5$  and  $3.4 \pm 0.2$ , respectively, ie. lower than the physiological pH, so that both surfaces are negatively charged in the most common bacterial culture media (pH = 6.8-7.0).<sup>46</sup> This was confirmed by the experiment that showed that sessile *E. coli* bacteria were in similar amount on

---

P25 and PANaF coatings before any photocatalytic treatment. Damage and inactivation of bacteria observed with up to 45 min of treatment should be thus attributed to photocatalysis, i.e. the physico-chemical properties of the TiO<sub>2</sub> photocatalysts or of the coatings.

PANaF TiO<sub>2</sub> is expected to perform better than the P25 TiO<sub>2</sub> reference for many different aspects. XRD patterns revealed that the PANaF TiO<sub>2</sub> powders had a smaller mean crystallite size than the P25 TiO<sub>2</sub> reference (about 10-11 nm vs. 22 nm for the anatase phase in P25) (Figure 3), associated to its higher specific surface area (130 m<sup>2</sup>/g vs. 55 m<sup>2</sup>/g). The results were confirmed by TEM analysis, for PANaF and P25 TiO<sub>2</sub> powders (with a 12-15 nm mean crystallite size vs. 22-25 nm, respectively). It was shown that this fine-tuned material morphology directly results from the use of phosphoric acid (PA) and sodium fluoride (NaF) additives in a P/F-assisted sol-gel synthesis of TiO<sub>2</sub>. Thanks to the use of both additives, a much higher photocatalytic activity in the gas-phase methyl ethyl ketone degradation was obtained with PANaF TiO<sub>2</sub> in comparison to P25. Indeed, the number of adsorption and reaction surface sites was increased and an improvement of the photogenerated electron-hole charge flow separation was proposed, which reduces the charge recombination rate.<sup>35</sup> Here as well, the increased number of surface sites favors the production of ROS, and consequently the subsequent antibacterial effect in aqueous phase.

Besides, the surface topographic properties are likely to provide some advantage to the PANaF coating over its P25 counterpart. As measured by AFM and reported in Figure 4, strong differences in surface roughness and morphology are noticed: the surface of the P25 coating is composed of large grain-like convex structures with size of  $180 \pm 35$  nm, while the PANaF coating surface is smoother (mean lateral particle size of 75 nm vs. 120 nm for PANaF and P25, respectively) and the grain size is smaller ( $42 \pm 16$  nm). This is consistent with the smaller TiO<sub>2</sub> crystal size of PANaF compared to P25. Indeed, even though the observed grains are probably aggregates rather

---

than single crystals, smaller crystals are expected to form smaller aggregates than larger crystals do, if the form of primary particles is non-anisotropic. This has been especially shown for aggregates of P25 and of smaller size sol-gel TiO<sub>2</sub>.<sup>47</sup> This difference in topography does not result in different surface coverage by bacteria of the coatings as shown before UV-A illumination (Figure S4). However, the photocatalytic effect on adhered bacteria might be impacted. Due to their large size (1-3 μm) compared to the TiO<sub>2</sub> aggregates, bacterial cells lie on the coating's surface with only a limited numbers of contact points.<sup>48</sup> On PANaF coatings, the smoother topography results in a higher number of contact points with shallower valleys in between. This is beneficial to the photocatalytic activity,<sup>49</sup> since the reactive generated ROSs need to diffuse for a shorter distance to reach the target i.e. the bacterium at the surface of the PANaF coating compared to the P25 coating (Figure 4), which has been reported to prevent dramatic loss of the ROSs.<sup>50</sup>

### **Longer-term, biofilm-preventive antibacterial effect**

Bacteria's fate on the coatings after treatment by photocatalysis has been investigated. Adhered *E. coli* were allowed to recover for 16 h in favorable growth conditions after different photocatalytic treatment times. Their amounts after the recovery period are depicted in Figure 5 and Figure S11, and some typical micrographs are shown in Figure S12. As expected, the surface coverage by "Live" bacteria without photocatalytic treatment increased from 15-20 % to up to 40-50 % on the TiO<sub>2</sub> coatings after overnight culture in nutrition-rich conditions. In contrast, the surface coverage increased from nearly 0% when a prior UV-A treatment was applied for 10 min or 45 min to 15-20 % on both P25 and PANaF coatings after overnight culture. Overall, the longer-term antibacterial effect of the TiO<sub>2</sub> coating is able to limit the bacterial overnight regrowth to roughly 60% of surface coverage relative to that on a non-treated coating (Figure 5 B). This demonstrates that the few "Live" bacterial cells still adhered on the coatings after photocatalytic treatment

---

(Figure 1C) were able to grow if placed in favorable conditions. However, only few bacteria that were damaged by the treatment were able to recover, as suggested by the similar fraction of bacteria remaining “Damaged” (i.e. red) after the overnight culture (10%) (Figure 5 A) compared to the fraction measured directly after the photocatalytic treatment (10-20%) (Figure 1 C).

### **3.3. Variations of the photocatalytic antibacterial performance with bacterial species**

The photocatalytic antibacterial performance, regarding both immediate and longer-term effects, was expected not to depend only on the material and the coating properties, but also on the bacterial species mainly due to strong differences in resistance to oxidative stress. Investigation conducted with *S. epidermidis* ATCC 35983 (CIP 106510) and *P. fluorescens* ATCC 13525 (CIP 69.13T) strains on the PANaF and P25 coatings revealed significant differences in the photocatalytic effect compared to the results observed with *E. coli*.

With *S. epidermidis* ATCC 35983 (CIP 106510), the results reveal a strong reduction of the “Live” bacteria quantity on both the coatings after 45 min UVA illumination (Figure 6 A, Figure S13 and Figure S14 for micrograph examples). However, 10 min UVA treatment failed to cause any antibacterial effect on P25 coating and only a slight advantage of PANaF coating was evidenced with “Live” bacteria quantity being reduced to about 80% of the initial population. 10 min UVA treatment also failed to provide any antibacterial effect on *P. fluorescens* ATCC 13525 (CIP 69.13T) strain on the P25 coating, but also on the PANaF coating (Figure 6 B and Figure S15). Nevertheless, 45 min UVA illumination led to a significant reduction of the “Live” bacteria quantity on both P25 and PANaF coatings, but the reduction was only of about 70% on the PANaF coating and 50% on the P25 coating, thus not as efficient as with *E. coli*. In addition, as illustrated

---

in confocal micrographs (Figure S16), some bacterial cells were stained as dark orange instead of red, which is the result from double cell staining by red PI and green Syto9®. This indicates that the cell wall integrity was affected, even though damages were not strong enough to allow PI to completely replace Syto9® in DNA. Longer UVA treatment, tested for up to 3 h illumination, did not result in any further improvement of the antibacterial effect as seen in Figure 6 B.

After overnight growth in nutrient-rich culture medium without any previous treatment, *S. epidermidis* population that initially covered about 10% surface of the coatings grew to about 50% coverage in absence of photocatalytic treatment (comparison between Figure S15 and Figure S17). With a previous 10 min UVA treatment, the bacterial population was unchanged (49% and 50% on P25 and PANaF coatings respectively) (Figure 6 C, Figure S17 and Figure S18). However, with 45 min UVA illumination, longer-term growth was significantly reduced, the coverage by “Live” bacteria being lowered to 40% of the P25 coating and about 30% of the PANaF coating. “Damaged” bacteria quantity was almost unchanged after the overnight growth in favorable conditions compared to immediately after the photocatalytic treatment, which suggests that damaged bacteria were mainly unable to recover, similarly to that observed with the *E. coli* SCC1 strain. Thus, photocatalytic treatment of *S. epidermidis* on both P25 and PANaF TiO<sub>2</sub> coatings was able to inhibit the growth of a significant part of the sessile bacterial population even after a long recovery time in favorable conditions. In contrast, 45 min of treatment failed to avoid the formation of a thick *P. fluorescens* biofilm after post-treatment growth in nutritive medium (Figure S19) even though the micrographs suggest some moderate inhibition on both TiO<sub>2</sub> coatings (Figure S20). A more pronounced inhibition was achieved after 3 h illumination as evidenced by the much less dense “Live” bacterial biomass observed in the biofilm. In addition, “damaged” bacteria were in higher quantity on the PANaF coating than on the P25 one.

---

Finally, bacterial species are ranked as following in terms of their rate of inactivation after the same photocatalytic treatment on the same TiO<sub>2</sub> coating: *E. coli* > *S. epidermidis* > *P. fluorescens*, from the most to the least sensitive. Indeed, the possible effect of differences in adhesion rate between species is rejected since the inactivation rate relates to the number of adhered bacteria of each species measured without treatment. Therefore, three species-related factors may be involved in this variation in sensitivity: 1) the production of extracellular matrix (ECM), 2) the structure properties of the bacteria cell wall and 3) the defense mechanism countering ROSs.

ECM is expected to form a screen that partially hides the TiO<sub>2</sub> nanocrystals from the irradiation beam.<sup>51</sup> It also probably acts as a diffusion barrier for ROSs that have been produced.<sup>52</sup> However, illumination treatments were all carried out on bacteria just adhered (3 h of incubation) in physiologic saline solution, which is not expected to conduct to the formation of a significant biofilm.<sup>53</sup> Hence, ECM is here expected not to have been produced in a sufficient quantity to compromise the photocatalysis effect.

Bacteria's cell wall type might also vary the bacterial susceptibility to ROSs. Indeed, both outer membrane and peptidoglycan (PGN) layers, which are the main barriers for ROSs before damaging the cytoplasmic membrane, differ with Gram-negative / Gram-positive class of bacteria (Figure 7).<sup>54</sup> Lipopolysaccharide and lipid layers of the outer membrane of Gram-negative bacteria have been demonstrated to be easily degraded through photocatalysis.<sup>55-56</sup> In contrast, the PGN layer, that is much thicker in Gram-positive bacteria, was shown to be the most resistant component of the cell wall.<sup>57</sup> However, the natural pores of the PGN layer are large enough for the diffusion (bypass) of ROSs (if live long enough) in the absence of any PGN degradation.<sup>54</sup> Therefore, variation of sensitivity based on the typical cell wall composition associated to the Gram-positive and versus Gram-negative classification is not obvious. This is in agreement with

---

the literature that failed to report direct correlation between photocatalytic antibacterial efficacy and the cell wall type so far.<sup>58</sup>

Whatever the cell wall type, ROSs finally reach the cytoplasmic membrane. There, vital metabolic functions such as enzymatic and respiratory activities may be affected.<sup>42, 59</sup> This is therefore the ultimate and the most vital defensive line against many environmental stresses<sup>60</sup>. In our study, adhered *E. coli* cells with active enzymatic and respiratory activities were still in high number on both TiO<sub>2</sub> coatings after 45 min of UVA treatment, although their GFP production, which signs the metabolic activity, was shown to be almost completely inactivated. Their cell wall was also almost completely damaged. In addition, the enzymatic activity was less reduced than the respiratory activity. This confirms that ROSs attacked the cytoplasmic membrane as first, which is the location of *E. coli* respiratory, while the remaining quantity of ROSs reached then the cytoplasm (Figure 7). In the bacterial cell cytoplasm, all three bacteria used in the present work had catalase and SOD, two important anti-oxidative enzymes providing defenses against ROSs. However, their capacity to inhibit ROSs varies with species.<sup>61</sup> Facultative anaerobic *S. epidermidis* and *E. coli* bacteria are more sensitive to oxygen exposure than aerobic organisms that have moved towards intricate mechanisms to neutralize ROSs.<sup>62-64</sup> Thus, Alhasawi *et al.* have demonstrated that an obligate aerobic wild *P. fluorescens* strain can survive in media with 500 μM H<sub>2</sub>O<sub>2</sub> by generating NADPH, ATP and glyoxylate in an effort to fend off ROSs.<sup>31</sup> This pronounced difference in fighting against ROSs is the probable main cause of the difference in sensitivity to the photocatalytic treatment observed between *E. coli* and *S. epidermidis* on the one side and *P. fluorescens* on the other side. In addition, *E. coli* K12 strains such as *E. coli* SCC1 lack one of the SODs compared to environmental *E. coli* B strain. This allows us to suggest that *E. coli* SCC1

---

bacteria exhibit less resistance to ROSs in comparison to *S. epidermidis* and *P. fluorescens* bacteria, *P. fluorescens* being the most resistant due to adequate adaptation to aerobic conditions.

### **3.4. Influence of oxygen and ions on the photocatalytic antibacterial performance**

Environmental factors such as the oxygen level and the presence of ions in the reaction medium are prone to strongly affect the photocatalytic antibacterial effects. We therefore investigated the immediate photocatalytic antibacterial effect in a confined, *i.e.* O<sub>2</sub>-poor, environment (Figure 8) for *E. coli* SCC1 strain on both P25 and PANaF coatings. The surface fraction covered by bacteria without treatment was low (2%-5%) in agreement with the low bacteria's quantity inoculated on the surface in the confined environment (only 20 µl of bacteria suspension). After a 45 min UVA treatment, neither P25 nor PANaF coating revealed any significant reduction in the quantity of "Live" bacteria, which is in a great contrast with the results obtained in the "open" aerated system used for the above reported results (Figure 1 B). The lack of significant photocatalytic activity on the confined TiO<sub>2</sub> coatings was confirmed after 3 h UVA illumination (data not shown). Noticeably, the lack of antibacterial effect was associated with a color change of the TiO<sub>2</sub> coatings (Figure S21). Typically, the coating revealed white color in aerated conditions, which was unchanged after illumination. Placed in the confined environment, the coating turned from white to a bluish color, regardless of the concentration of bacteria used for the inoculation, which is attributed to the formation of reduced TiO<sub>2</sub> (Ti<sup>3+</sup>) with the formation of oxygen vacancies.<sup>65-66</sup> By using an oxygen sensor patch, an immediate and strong decrease in the level of dissolved oxygen was actually revealed by a sharp boost of fluorescence intensity upon UVA illumination in the confined condition (Figure 9). In contrast, the red fluorescence intensity was much lower upon illumination in aerated conditions, as well as in the absence of illumination in both aerated or

---

confined environments, as expected for oxygen-rich media. The low level of oxygen content in the confined environment might lead to the impossibility for photogenerated electrons to be evacuated through the usual reduction of adsorbed O<sub>2</sub> molecules.<sup>67</sup> Hence, the photogenerated electrons accumulate in the TiO<sub>2</sub> material, thus reducing Ti<sup>4+</sup> species into Ti<sup>3+</sup> centers as expected from the redox potential level of Ti<sup>3+</sup> lower than that of anatase TiO<sub>2</sub>.<sup>66</sup> The resulting TiO<sub>2</sub> structural changes alter the photocatalytic properties.<sup>66</sup> Besides, the lack of oxygen prevents any free-radical-induced chain scission of (bio)polymers,<sup>68</sup> which results in the preservation of biopolymers and therefore survival of bacteria upon photocatalytic treatment. Importantly, the presence of bacteria did not enhance the color change despite the O<sub>2</sub> uptake by bacteria for their respiratory activity, probably due to their low consumption of O<sub>2</sub> especially in a non-nutritive medium (NaCl 9 g/L).<sup>42</sup> It should be noticed that the blue color was more intense in the liquid freshly sterilized by autoclave just before use (e.g. physiological saline water), which is attributed to the removal of the dissolved oxygen. Finally, reduction of Ti<sup>4+</sup> into colored Ti<sup>3+</sup> is a non-material-dependent phenomenon that occurred similarly on both TiO<sub>2</sub> coatings.

Some ions in the reaction medium were also shown to influence the photocatalytic antibacterial effect. It was especially noticed that 1 h of photocatalytic treatment in M63G medium failed to result in any significant reduction in the “Live” bacteria’s quantity on both TiO<sub>2</sub> coatings (Figure 10), which is very different from the effect in physiological saline medium (Figure 1 B). Complementary experiment of the liquid phase photocatalytic degradation under UVA of methylene blue on the PANaF coatings in the presence or absence of M63G medium confirmed that the M63G medium inhibited the photocatalytic reaction (cf. Figure S22 and its description), even with a M63G medium diluted by 100 times with saline solution. XPS surface analysis (Table S1, Figure S23) revealed the characteristic doublet of P 2p<sub>3/2-1/2</sub> orbitals for non-polymerized

---

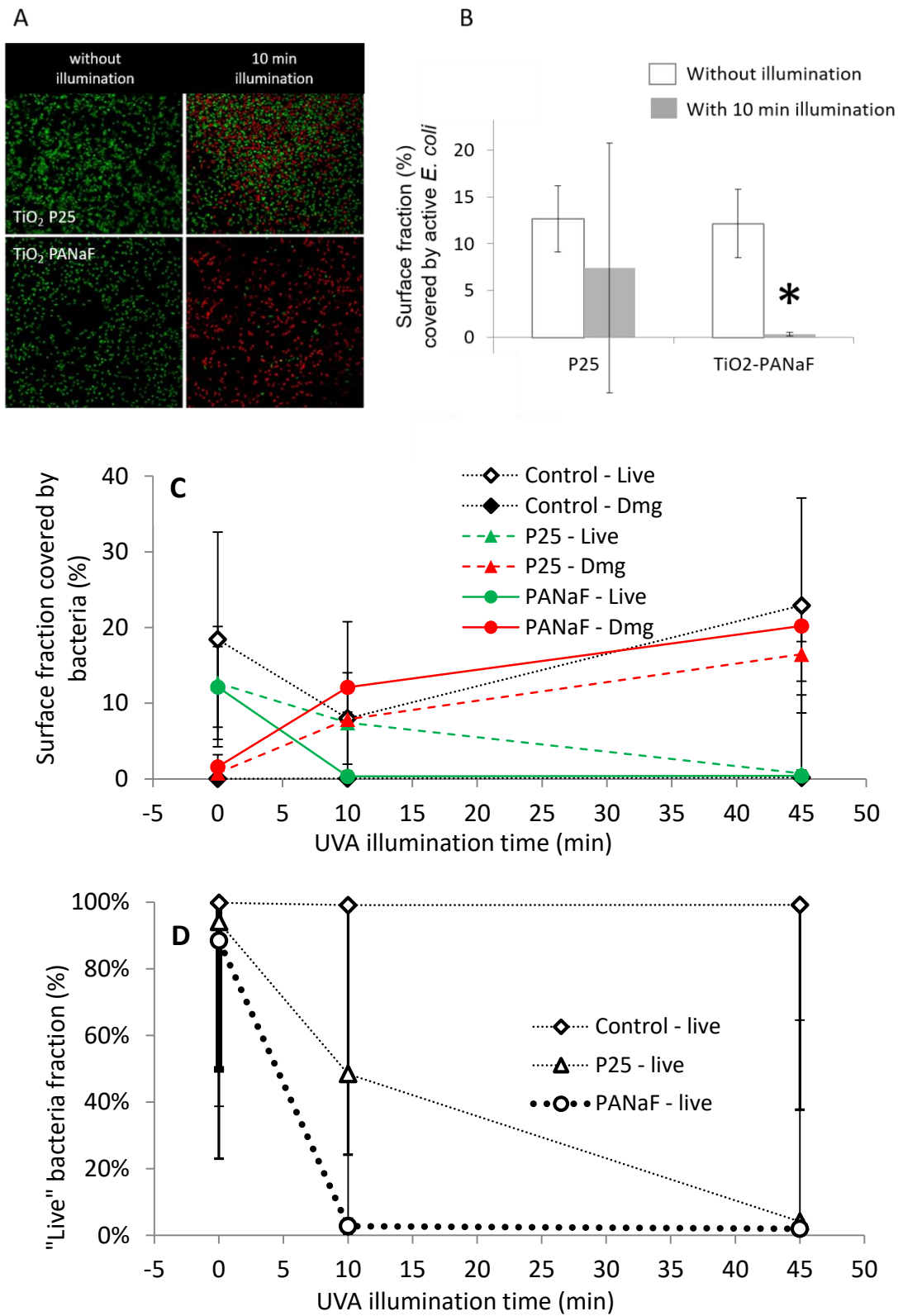
phosphate species (133.6 eV and 134.5 eV) in the case of the PANaF coating, as the expected consequence of using phosphoric acid as additive for the TiO<sub>2</sub> synthesis<sup>35</sup>, while logically no phosphorous was observed in the case of P25 coating (data not shown). After immersion in M63G medium, the P/Ti surface atomic ratio strongly increased for both TiO<sub>2</sub> coatings (Table S1), with the appearance of an additional P 2p<sub>3/2-1/2</sub> orbital doublet contribution (Figure S23 A, C) similar to that observed on TiO<sub>2</sub>-based composites used to adsorb phosphate from wastewater.<sup>69</sup> The presence of phosphate deposit was here attributed to phosphate adsorbed from the medium to the coating's surface. It was consequently the probable cause for the suppression of the photocatalytic antibacterial effect. Indeed, Rincon *et al.* reported that phosphate ion is the most detrimental compound among other common ions for the TiO<sub>2</sub> photocatalytic antibacterial effect on *E. coli*. It acts as a poison for the photocatalyst by competing with the oxidizing radicals, by blocking the surface active sites of the photocatalyst<sup>27</sup>, and by further serving as a charge recombination center.

#### 4. Conclusion

Photocatalytic antibacterial investigation was conducted under UVA irradiation on a heavy-metals-free P/F-modified TiO<sub>2</sub> coating against several bacterial species in comparison to a reference TiO<sub>2</sub>-P25 coating. In general, near-total inactivation of *E. coli* and *S. epidermidis* was obtained, with a clear of both nature and topography of the coating, and of illumination time. Significantly higher efficiency was achieved on the PANaF coating compared to its TiO<sub>2</sub>-P25 counterpart. Especially, the smaller size of the PANaF TiO<sub>2</sub> crystals lead to a smoother topography of the coating surface, which may reduce the diffusion length that the photogenerated ROSs must travel to attack the bacterial cell wall. For the first time on TiO<sub>2</sub> coatings, *in-situ* investigation of

---

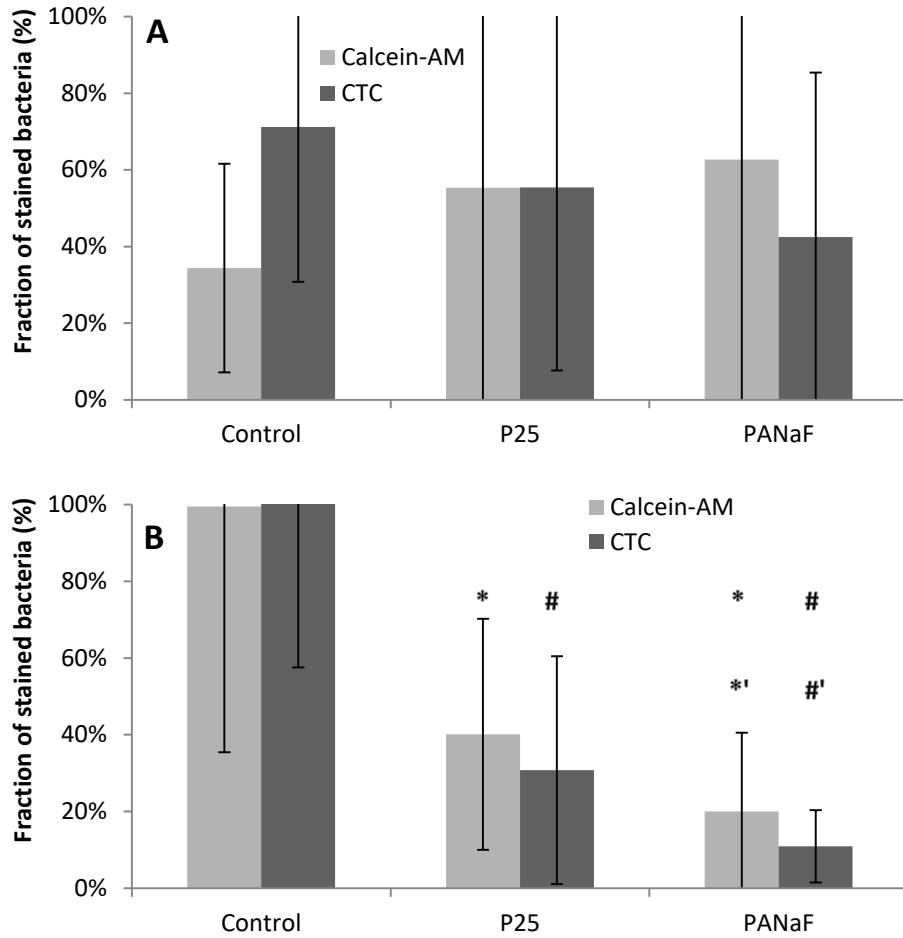
the cell wall integrity as well as of the respiratory and intracellular esterase activities showed that the photocatalytic treatment acts on the bacterial cells by attacking the successive barriers of the cell structure, with a decreasing photocatalytic effect as ROSs progress through the cell. Besides, we have evidenced a longer-term, biofilm-preventive effect on *E. coli* and *S. epidermidis* species in good correlation with the immediate photocatalytic antibacterial effect, while complete inactivation was not achieved with *P. fluorescens*, probably due to the capacity of *P. fluorescens* to fight the ROS-induced oxygen stress. In addition, the adsorption of phosphate ions on the TiO<sub>2</sub> surface and the lack of dissolved oxygen in the reaction medium are detrimental to the photocatalytic activity.



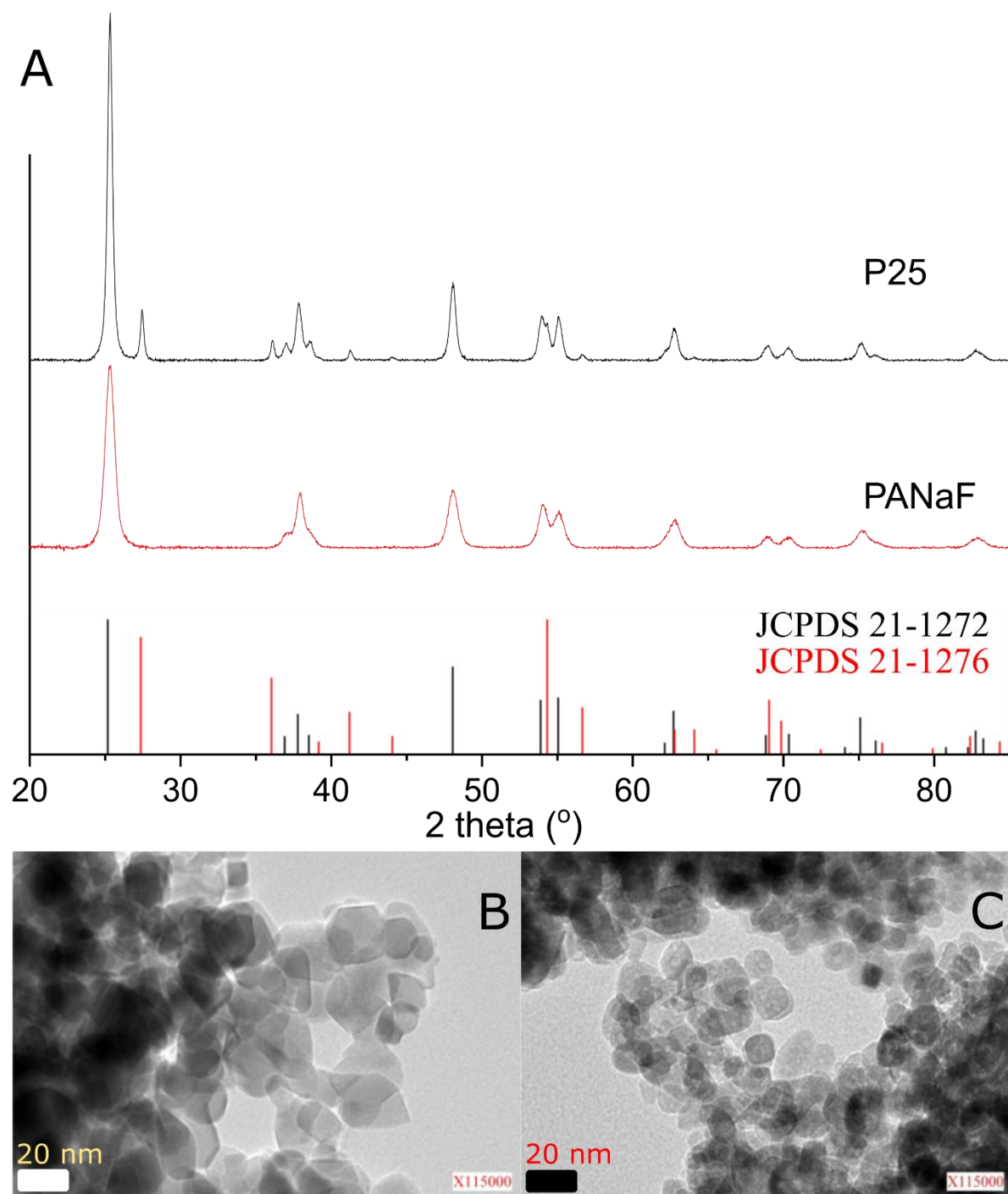
**Figure 1.** (A) Example of fluorescent images of *E. coli* SCC1 bacteria on P25 and PANaF coating

---

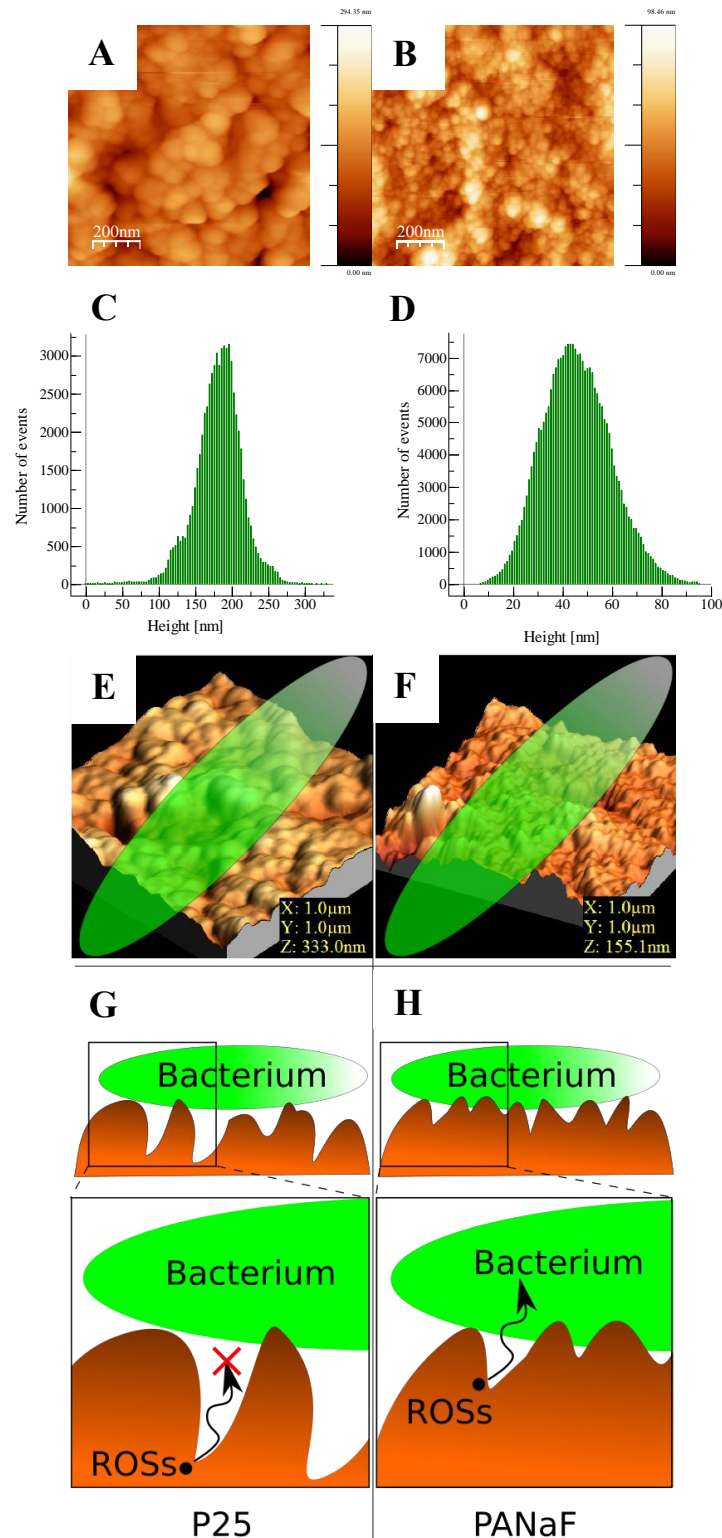
with and without 10 min of illumination. (B) Surface fraction covered by “Live” bacteria with and without 10 min of illumination on P25 and PANaF coating. (C) Surface fraction covered by “Live” (green) and “Damaged” (marked as “Dmg”) (red) bacteria and (D) fraction of “Live” bacteria in the population of *E. coli* SCC1 as a function of the illumination time on reference, P25 and PANaF coatings. Differences compared to t=0 are significant (p-value < 0.05) at all illumination length on P25 and PANaF coatings (cf. also in Figure S6).



**Figure 2.** CAM and CTC stained *E. coli* PHL 628<sup>41</sup> quantities for the reference, P25 and PANaF coatings after (A) 10 min and (B) 45 min of UVA illumination. \*: Significant differences in CAM stain (p-value < 0.05) compared to “Control”. #: Significant differences in CTC stain (p-value < 0.05) compared to “Control”. \*': Significant differences in CAM stain (p-value < 0.05) compared to “P25”. #' : Significant differences in CTC stain (p-value < 0.05) compared to “P25”.



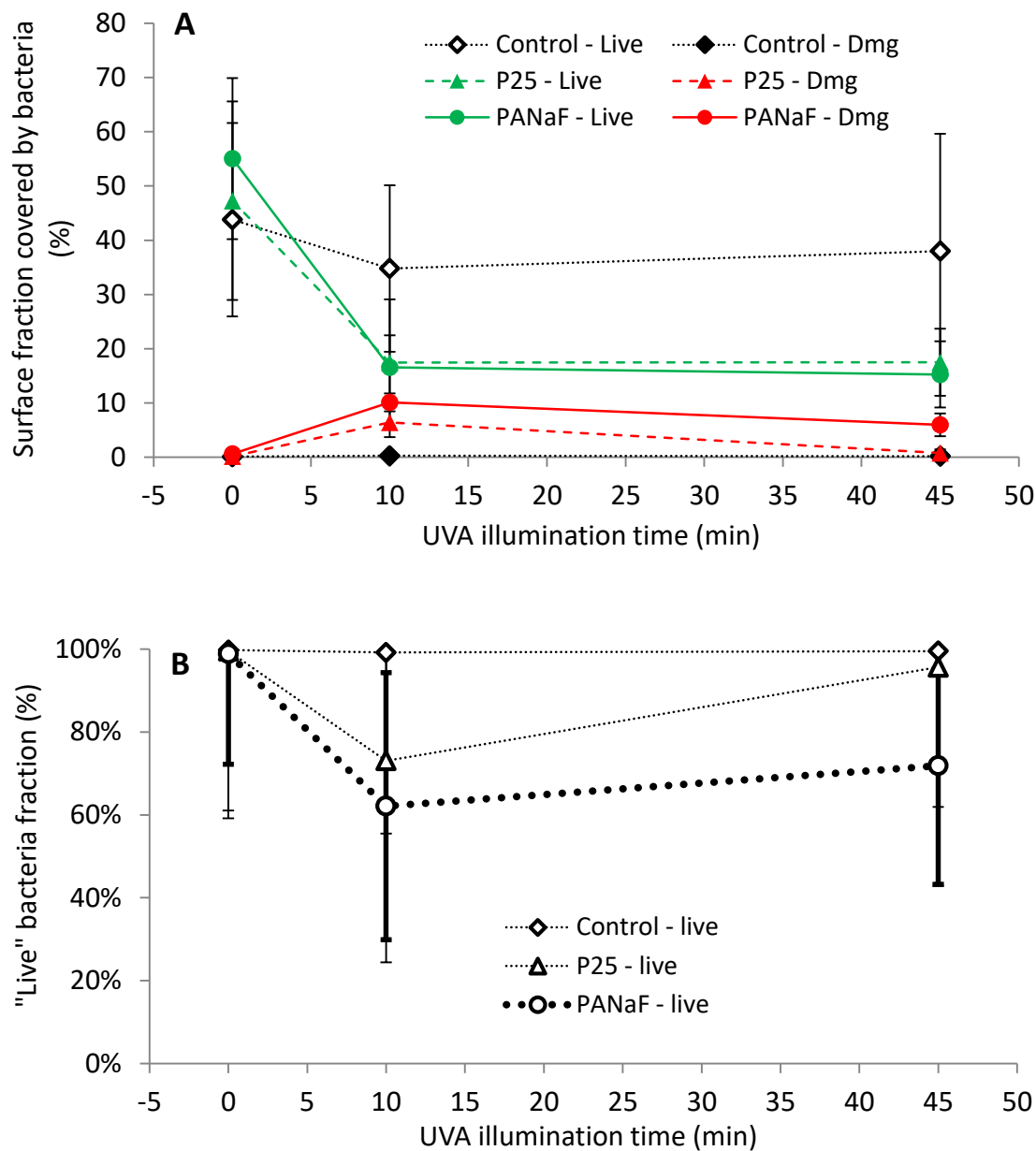
**Figure 3.** (A) XRD patterns of TiO<sub>2</sub> P25 and TiO<sub>2</sub> PANaF. The peak positions and relative intensities for TiO<sub>2</sub> anatase phase (black lines) and rutile phase (red lines), according to the JCPDS cards 21-1272 and 21-1276 respectively, are shown in the bottom of the frame. TEM images of (B) TiO<sub>2</sub> P25 and (C) TiO<sub>2</sub> PANaF powder samples.



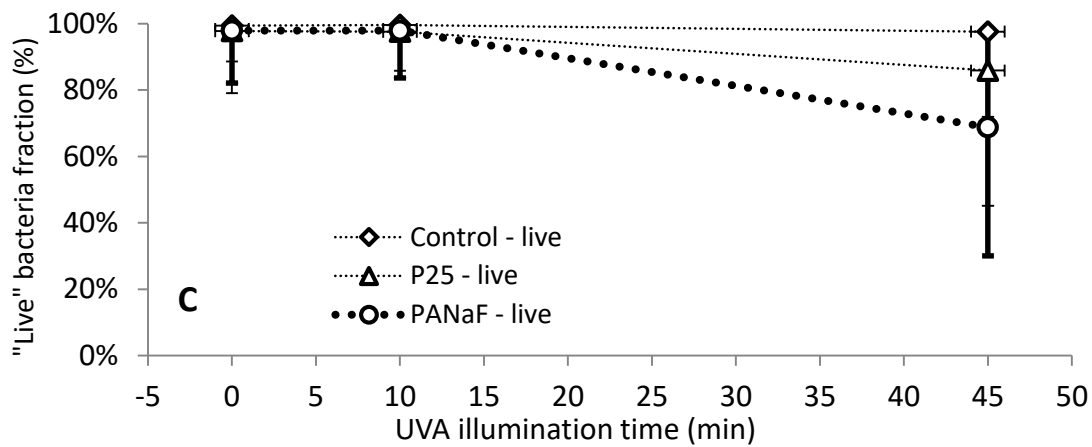
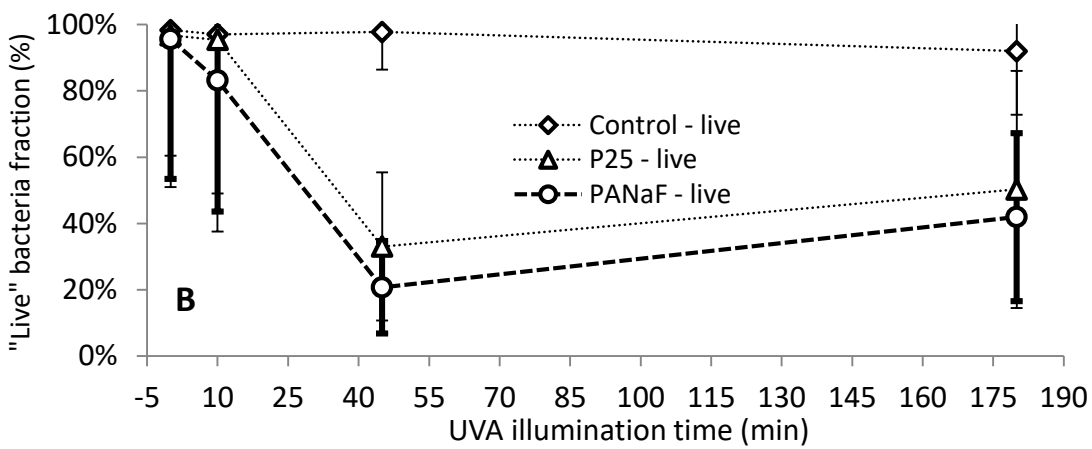
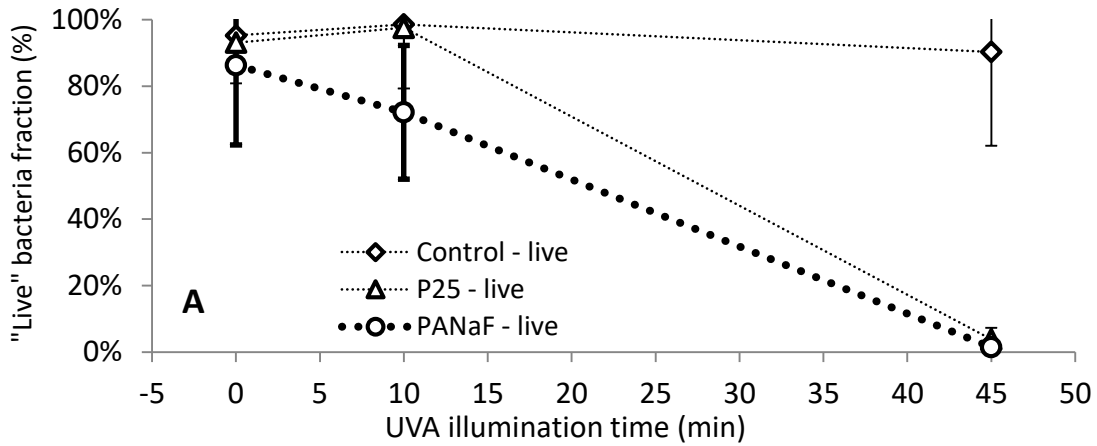
**Figure 4.** (A) Topological micrographs and (C) height profiles of the TiO<sub>2</sub> P25 coating, and (B, D) similar analysis performed on the TiO<sub>2</sub> PANaF coating surfaces, determined by AFM. 3D visualization of the surface topography of the (E) P25 and (F) PANaF TiO<sub>2</sub> coating, with the green

---

eclipse representing a single bacterium that is shown to scale. Schematic illustration of the contact between one bacterium and both (G) P25 TiO<sub>2</sub> and (H) PANaF coatings, and of the diffusion pattern of ROSs depending on the TiO<sub>2</sub> coating.



**Figure 5.** (A) Surface fraction covered by “Live” (green) and “Damaged (marked as Dmg)” (red) bacteria and (B) “Live” bacteria fraction of *E. coli* SCC1 after overnight growth in nutritive medium, as a function of the illumination time on control, P25 and PANaF coatings. Significant differences ( $p$ -value  $< 0.05$ ) are true compare to  $t=0$  at all illumination length on P25 and PANaF coatings (cf. student study in Figure S13).



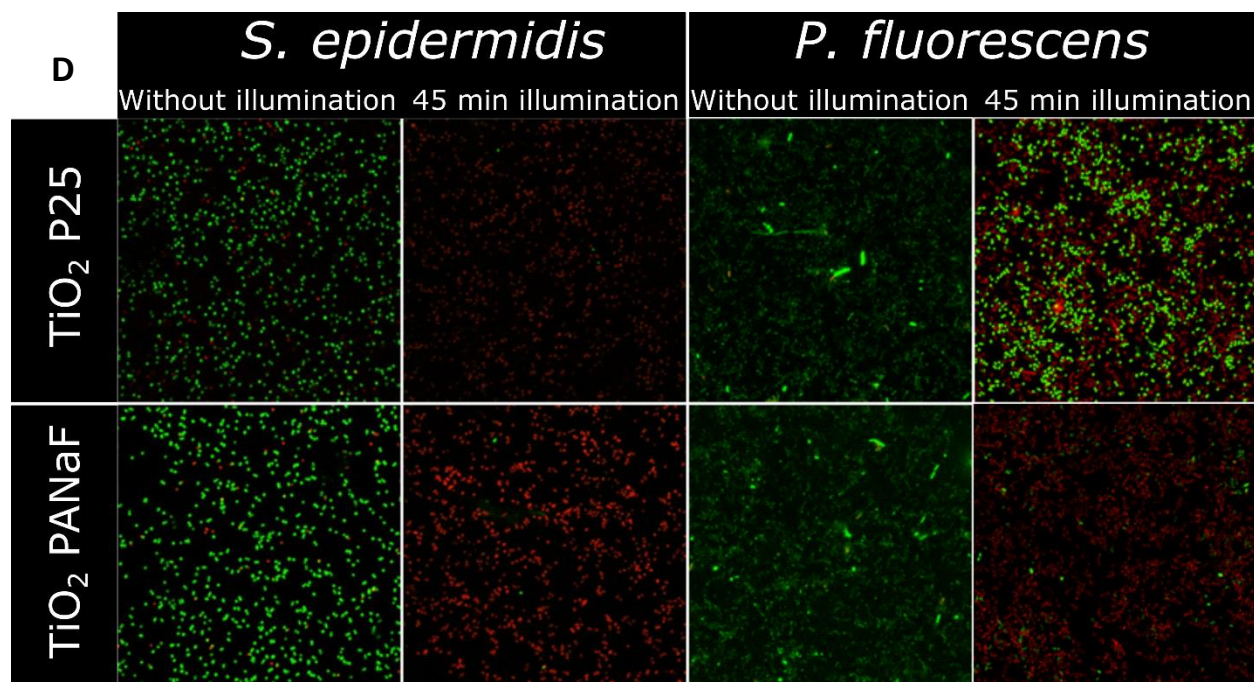


**Figure 6.** Fraction of “Live” bacteria after immediate photocatalytic treatment in the population of (A) *S. epidermidis* ATCC 35983 and (B) *P. fluorescens* ATCC 13525 strains as a function of the illumination time on control, P25 and PANaF coatings. Differences with  $t=0$  are significant ( $p$ -value  $< 0.05$ ) at all illumination length on P25 and PANaF coatings (cf. Figures S10 and S11). (C) Fraction of “Live” bacteria in the population of *S. epidermidis* ATCC 35983 (CIP 106510) after overnight growth in nutritive medium, as a function of the previous illumination time on control, P25 and PANaF coatings. Differences with  $t=0$  are significant ( $p$ -value  $< 0.05$ ) at 45min illumination length on P25 and PANaF coatings (cf. Figure S15). (D) Example of fluorescent images of *S. epidermidis* and *P. fluorescens* bacteria on P25 and PANaF coating with and without 45 min of illumination.

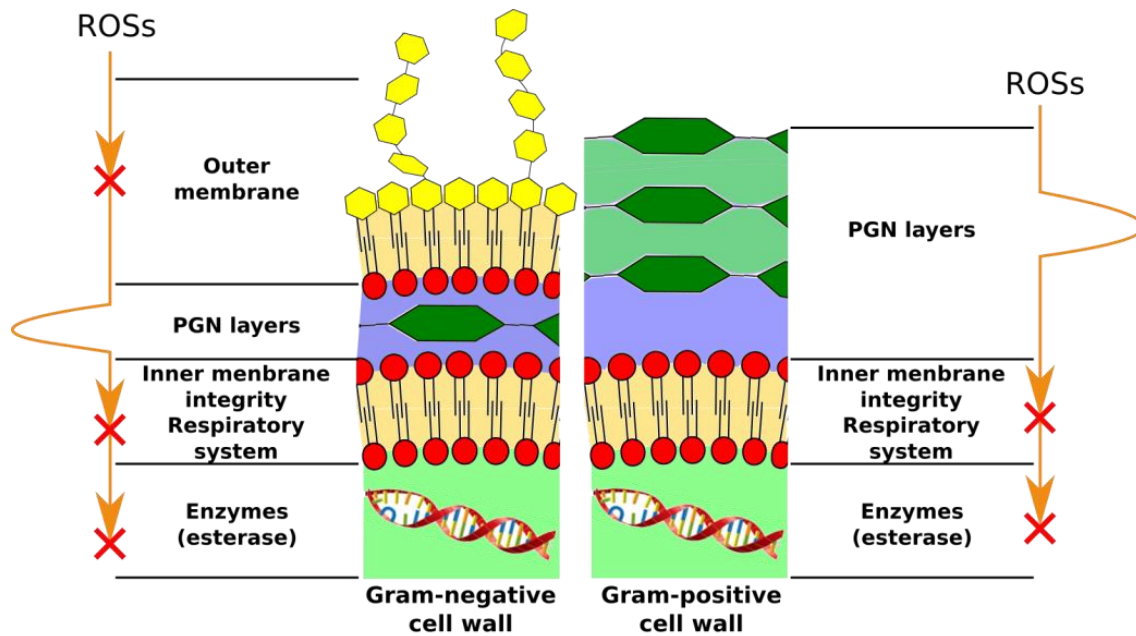


**Figure 7.** Illustration of the attack on the Gram-positive and Gram-negative bacteria cell wall by ROSs. The red crossovers from top to bottom represent the cell wall targets to be attacked by the photocatalytically generated ROSs. The detour around PNG layers means that ROSs do not easily degrade it but may bypass this layer thanks to pores.

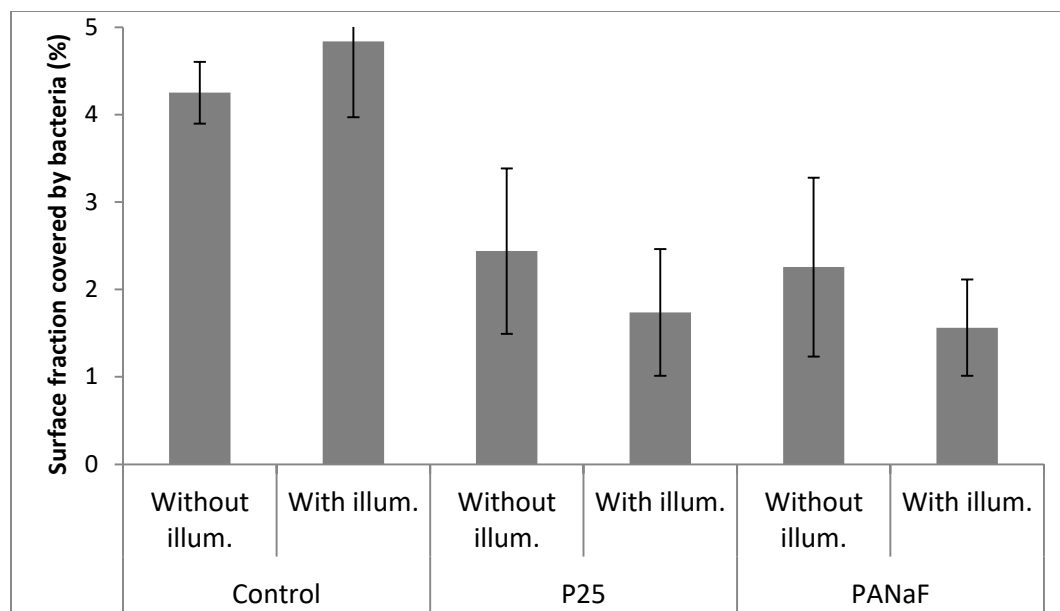


**Figure 8.** Immediate photocatalytic antibacterial effect on “Live” *E. coli* SCC1 bacteria adhered on the reference, P25 or PANaF coatings in a confined (oxygen-poor) environment, and with or without UVA illumination for 45 min. No significant differences ( $p$ -value  $< 0.05$ ) noticed between “Live” with or without 45 min of illumination on each coating.

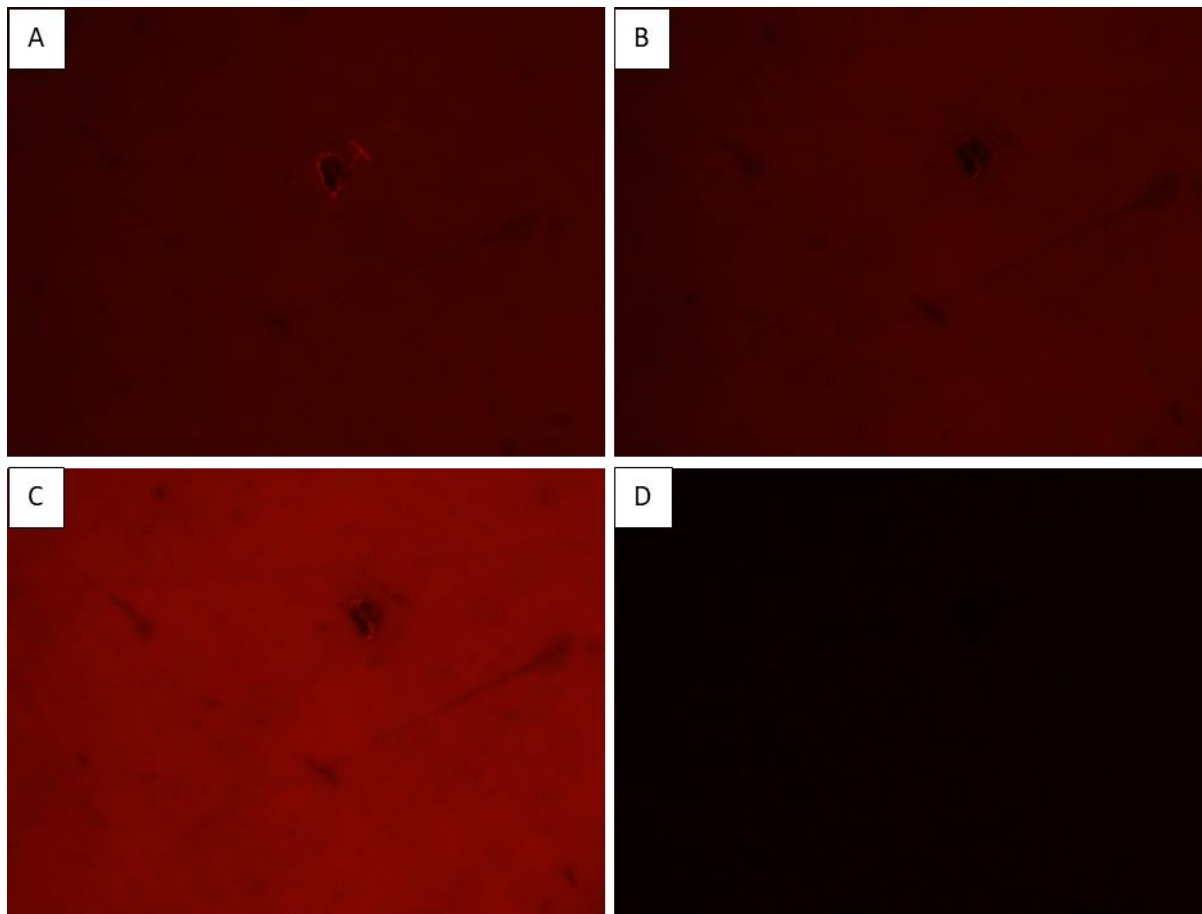


**Figure 9.** Fluorescent confocal images of an oxygen sensor patch in contact with a PANaF coating (A) in aerated condition, (B) in confined environment within physiological NaCl 9 g/L medium before UVA illumination, and (C) in confined environment within physiological NaCl 9 g/L medium during UVA illumination. (D) Fluorescence background (i.e. control condition) without any microscope laser excitation but with UVA illumination, showed uniform black color. The four photographs were taken at the same sample location.

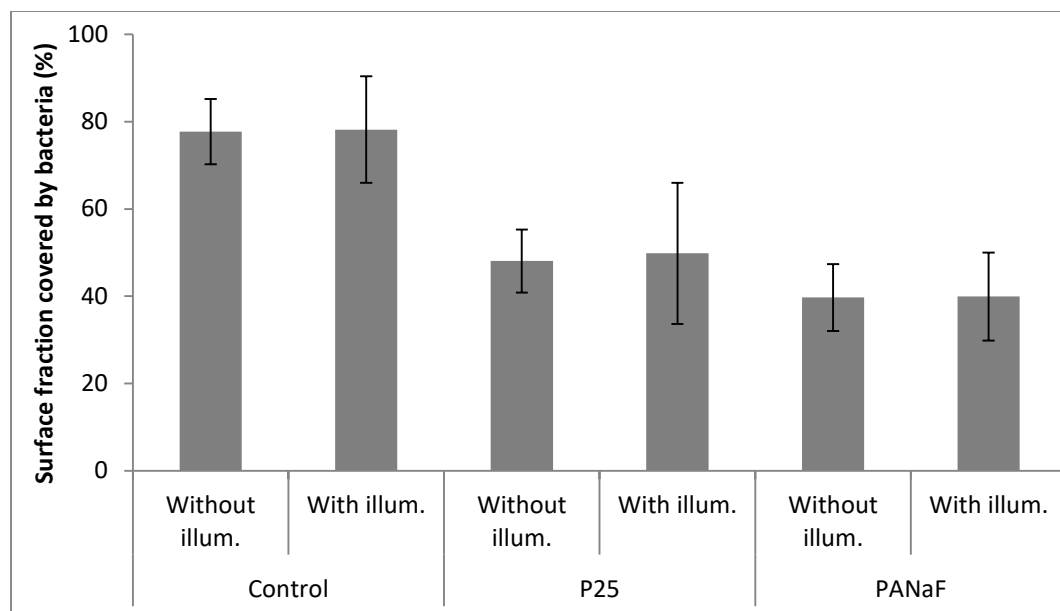


**Figure 10.** Immediate photocatalytic antibacterial effect on *E. coli* SCC1 species cultivated in M63G medium <sup>70</sup> on P25 and PANaF coatings and with or without 1 h of illumination. No significant differences (p-value < 0.05) are noticed for each coating with or without 1 h of illumination.

---

**Supporting Information.** Examples of fluorescent images of bacteria, surface coverage by staining-positive bacteria, supplementary experimental information on studying the effect of phosphate ions adsorption and the lack of oxygen dissolved in the reaction medium on the photocatalytic bactericidal activity of TiO<sub>2</sub> coating.

### **Author contribution**

Yige Yan synthesized the photocatalysts and carried out most of the tests, he also co-designed certain auxiliary experiments on studying the effects of phosphate ions adsorption and the dissolved oxygen concentration on the photocatalytic bactericidal activity of TiO<sub>2</sub> coating. Charline Soraru contributed partially to the microbiological studies.

### **Corresponding Author**

\* Corresponding author: Dr Lydie Ploux, [ploux@unistra.fr](mailto:ploux@unistra.fr), +33 (0)368855479

BioMaterials and BioEngineering, U1121

11 rue Humann 67000 Strasbourg

France

### **Funding Sources**

This work is part of CLEANCOAT project funded by the MICA CARNOT (Materials Institute Carnot Alsace).

---

## Acknowledgment

Dr A. Airoudj, Dr L. Vidal and Dr S. Garreau (IS2M) are thanked for the AFM, TEM and XPS measurements respectively. We acknowledge CRT Aériale (Illkirch, France) for its assistance in complementary microbiological tests.

## REFERENCES

- (1) Ploux, L.; Ponche, A.; Anselme, K. Bacteria/material interfaces: role of the material and cell wall properties. *Journal of Adhesion Science and Technology* **2010**, *24* (13-14), 2165-2201, DOI: 10.1163/016942410x511079.
- (2) Song, R.; Zhang, Y.; Huang, Q.; Yang, Y.; Lin, L.; Liang, J.; Hu, R.; Rui, G.; Lin, C. Facile Construction of structural gradient of TiO<sub>2</sub> nanotube arrays on medical titanium for high throughput evaluation of biocompatibility and antibacterial property. *ACS Applied Bio Materials* **2018**, *1* (4), 1056-1065, DOI: 10.1021/acsabm.8b00288.
- (3) Capita, R.; Alonso-Calleja, C. Antibiotic-resistant bacteria: a challenge for the food industry. *Critical Reviews in Food Science and Nutrition* **2013**, *53* (1), 11-48, DOI: 10.1080/10408398.2010.519837.

- 
- (4) Liu, S.; Gunawan, C.; Barraud, N.; Rice, S. A.; Harry, E. J.; Amal, R. Understanding, monitoring, and controlling biofilm growth in drinking water distribution systems. *Environmental Science & Technology* **2016**, *50* (17), 8954-8976, DOI: 10.1021/acs.est.6b00835.
- (5) Rizzo, L.; Manaia, C.; Merlin, C.; Schwartz, T.; Dagot, C.; Ploy, M. C.; Michael, I.; Fatta-Kassinos, D. Urban wastewater treatment plants as hotspots for antibiotic resistant bacteria and genes spread into the environment: A review. *Science of The Total Environment* **2013**, *447*, 345-360, DOI: <https://doi.org/10.1016/j.scitotenv.2013.01.032>.
- (6) Tsibouklis, J.; Stone, M.; Thorpe, A. A.; Graham, P.; Peters, V.; Heerlien, R.; Smith, J. R.; Green, K. L.; Nevell, T. G. Preventing bacterial adhesion onto surfaces: the low-surface-energy approach. *Biomaterials* **1999**, *20* (13), 1229-1235.
- (7) Weber, D. J.; Rutala, W. A. Self-disinfecting surfaces: review of current methodologies and future prospects. *American journal of infection control* **2013**, *41* (5 Suppl), S31-5, DOI: 10.1016/j.ajic.2012.12.005.
- (8) Bakhsheshi-Rad, H. R.; Hamzah, E.; Ismail, A. F.; Aziz, M.; Daroonparvar, M.; Saebnoori, E.; Chami, A. In vitro degradation behavior, antibacterial activity and cytotoxicity of TiO<sub>2</sub>-MAO/ZnHA composite coating on Mg alloy for orthopedic implants. *Surface and Coatings Technology* **2018**, *334*, 450-460, DOI: <https://doi.org/10.1016/j.surfcoat.2017.11.027>.

- 
- (9) Rtimi, S.; Dionysiou, D. D.; Pillai, S. C.; Kiwi, J. Advances in catalytic/photocatalytic bacterial inactivation by nano Ag and Cu coated surfaces and medical devices. *Applied Catalysis B: Environmental* **2019**, *240*, 291-318, DOI: 10.1016/j.apcatb.2018.07.025.
- (10) Rutala, W. A.; Weber, D. J. New disinfection and sterilization methods. *Emerging infectious diseases* **2001**, *7* (2), 348.
- (11) Bonetta, S.; Bonetta, S.; Motta, F.; Strini, A.; Carraro, E. Photocatalytic bacterial inactivation by TiO<sub>2</sub> coated surface. *AMB Express* **2013**, *3*, 59.
- (12) Mills, A.; Le Hunte, S. An overview of semiconductor photocatalysis. *Journal of photochemistry and photobiology A: Chemistry* **1997**, *108* (1), 1-35.
- (13) Jacoby, W. A.; Maness, P. C.; Wolfrum, E. J.; Blake, D. M.; Fennell, J. A. Mineralization of bacterial cell mass on a photocatalytic surface in air. *Environmental Science & Technology* **1998**, *32* (17), 2650-2653.
- (14) Benabbou, A.; Derriche, Z.; Felix, C.; Lejeune, P.; Guillard, C. Photocatalytic inactivation of *Escherichia coli*: Effect of concentration of TiO<sub>2</sub> and microorganism, nature, and intensity of UV irradiation. *Applied Catalysis B: Environmental* **2007**, *76* (3), 257-263.
- (15) Kühn, K. P.; Chaberny, I. F.; Massholder, K.; Stickler, M.; Benz, V. W.; Sonntag, H.-G.; Erdinger, L. Disinfection of surfaces by photocatalytic oxidation with titanium dioxide and UVA light. *Chemosphere* **2003**, *53* (1), 71-77, DOI: 10.1016/s0045-6535(03)00362-x.

- 
- (16) Adamek, E.; Baran, W.; Ziemiańska-Błaszczyk, J.; Sobczak, A. Immobilisation of TiO<sub>2</sub>-P25 on a glass fibre mat: Preparation, photocatalytic activity and stability. *Solar Energy* **2019**, *188*, 1232-1242, DOI: 10.1016/j.solener.2019.07.034.
- (17) Barthomeuf, M.; Castel, X.; Le Gendre, L.; Louis, J.; Denis, M.; Pissavin, C. Effect of titanium dioxide film thickness on photocatalytic and bactericidal activities against *Listeria monocytogenes*. *Photochem Photobiol* **2019**, *95* (4), 1035-1044, DOI: 10.1111/php.13078.
- (18) Ganguly, P.; Byrne, C.; Breen, A.; Pillai, S. C. Antimicrobial activity of photocatalysts: Fundamentals, mechanisms, kinetics and recent advances. *Applied Catalysis B: Environmental* **2018**, *225*, 51-75, DOI: 10.1016/j.apcatb.2017.11.018.
- (19) Clemente, A.; Ramsden, J. J.; Wright, A.; Iza, F.; Morrissey, J. A.; Li Puma, G.; Malik, D. J. *Staphylococcus aureus* resists UVA at low irradiance but succumbs in the presence of TiO<sub>2</sub> photocatalytic coatings. *Journal of photochemistry and photobiology. B, Biology* **2019**, *193*, 131-139, DOI: 10.1016/j.jphotobiol.2019.02.009.
- (20) Ohtani, B.; Prieto-Mahaney, O. O.; Li, D.; Abe, R. What is Degussa (Evonik) P25? Crystalline composition analysis, reconstruction from isolated pure particles and photocatalytic activity test. *Journal of Photochemistry and Photobiology A: Chemistry* **2010**, *216* (2-3), 179-182, DOI: 10.1016/j.jphotochem.2010.07.024.

---

(21) van Grieken, R.; Marugán, J.; Sordo, C.; Martínez, P.; Pablos, C. Photocatalytic inactivation of bacteria in water using suspended and immobilized silver-TiO<sub>2</sub>. *Applied Catalysis B: Environmental* **2009**, *93* (1-2), 112-118, DOI: 10.1016/j.apcatb.2009.09.019.

(22) Karunakaran, C.; Abiramasundari, G.; Gomathisankar, P.; Manikandan, G.; Anandi, V. Preparation and characterization of ZnO–TiO<sub>2</sub> nanocomposite for photocatalytic disinfection of bacteria and detoxification of cyanide under visible light. *Materials Research Bulletin* **2011**, *46* (10), 1586-1592, DOI: <https://doi.org/10.1016/j.materresbull.2011.06.019>.

(23) Zahid, M.; Papadopoulou, E. L.; Suarato, G.; Binas, V. D.; Kiriakidis, G.; Gounaki, I.; Moira, O.; Venieri, D.; Bayer, I. S.; Athanassiou, A. Fabrication of visible light-induced antibacterial and self-cleaning cotton fabrics using manganese doped TiO<sub>2</sub> nanoparticles. *ACS Applied Bio Materials* **2018**, *1* (4), 1154-1164, DOI: 10.1021/acsabm.8b00357.

(24) Ploux, L.; Anselme, K.; Dirani, A.; Ponche, A.; Soppera, O.; Roucoules, V. Opposite responses of cells and bacteria to micro/nanopatterned surfaces prepared by pulsed plasma polymerization and UV-irradiation. *Langmuir : the ACS journal of surfaces and colloids* **2009**, *25* (14), 8161-9, DOI: 10.1021/la900457f.

(25) Yao, N.; Lun Yeung, K. Investigation of the performance of TiO<sub>2</sub> photocatalytic coatings. *Chem. Eng. J.* **2011**, *167* (1), 13-21, DOI: 10.1016/j.cej.2010.11.061.

(26) Zhang, S.; Liang, X.; Gadd, G. M.; Zhao, Q. Advanced titanium dioxide-polytetrafluorethylene (TiO<sub>2</sub>-PTFE) nanocomposite coatings on stainless steel surfaces with

---

antibacterial and anti-corrosion properties. *Applied Surface Science* **2019**, *490*, 231-241, DOI: 10.1016/j.apsusc.2019.06.070.

(27) Rincon, A. Effect of pH, inorganic ions, organic matter and H<sub>2</sub>O<sub>2</sub> on *E. coli* K12 photocatalytic inactivation by TiO<sub>2</sub> Implications in solar water disinfection. *Applied Catalysis B: Environmental* **2004**, *51* (4), 283-302, DOI: 10.1016/j.apcatb.2004.03.007.

(28) Kubacka, A.; Diez, M. S.; Rojo, D.; Bargiela, R.; Ciordia, S.; Zapico, I.; Albar, J. P.; Barbas, C.; Martins dos Santos, V. A.; Fernandez-Garcia, M.; Ferrer, M. Understanding the antimicrobial mechanism of TiO<sub>2</sub>-based nanocomposite films in a pathogenic bacterium. *Scientific reports* **2014**, *4*, 4134, DOI: 10.1038/srep04134.

(29) De Dicitillo, C. L.; Correa, M. G.; Martínez, F. B.; Streitt, C.; Galotto, M. J. Antimicrobial effect of titanium dioxide nanoparticles [Online]; *IntechOpen* **2020**, DOI: 10.5772/intechopen.90891. <https://www.intechopen.com/online-first/antimicrobial-effect-of-titanium-dioxide-nanoparticles> (accessed July 31, 2020).

(30) Bruno-Bárcena, J. M.; Azcárate-Peril, M. A.; Hassan, H. M. Role of antioxidant enzymes in bacterial resistance to organic acids. *Applied and environmental microbiology* **2010**, *76* (9), 2747-2753.

(31) Alhasawi, A.; Castonguay, Z.; Appanna, N. D.; Auger, C.; Appanna, V. D. Glycine metabolism and anti-oxidative defence mechanisms in *Pseudomonas fluorescens*. *Microbiological research* **2015**, *171*, 26-31, DOI: 10.1016/j.micres.2014.12.001.

- 
- (32) Koizumi, Y.; Yamada, R.; Nishioka, M.; Matsumura, Y.; Tsuchido, T.; Taya, M. Deactivation kinetics of *Escherichia coli* cells correlated with intracellular superoxide dismutase activity in photoreaction with titanium dioxide particles. *Journal of Chemical Technology and Biotechnology* **2002**, *77* (6), 671-677.
- (33) Gogniat, G.; Dukan, S. TiO<sub>2</sub> photocatalysis causes DNA damage via Fenton reaction-generated hydroxyl radicals during the recovery period. *Applied and environmental microbiology* **2007**, *73* (23), 7740-7743.
- (34) Rincón, A.; Pulgarin, C. Photocatalytical inactivation of *E. coli*: effect of (continuous–intermittent) light intensity and of (suspended–fixed) TiO<sub>2</sub> concentration. *Applied Catalysis B: Environmental* **2003**, *44* (3), 263-284.
- (35) Yan, Y.; Keller, V.; Keller, N. On the role of BmimPF<sub>6</sub> and P/F- containing additives in the sol-gel synthesis of TiO<sub>2</sub> photocatalysts with enhanced activity in the gas phase degradation of methyl ethyl ketone. *Applied Catalysis B: Environmental* **2018**, *234*, 56-69, DOI: 10.1016/j.apcatb.2018.04.027.
- (36) Jung, M. H.; Chu, M. J.; Kang, M. G. TiO<sub>2</sub> nanotube fabrication with highly exposed (001) facets for enhanced conversion efficiency of solar cells. *Chemical communications* **2012**, *48* (41), 5016-5018, DOI: 10.1039/c2cc31047c.
- (37) Doniach, S.; Sunjic, M. Many-electron singularity in X-ray photoemission and X-ray line spectra from metals. *Journal of Physics C: Solid State Physics* **1970**, *3* (2), 285.

- 
- (38) Shirley, D. A. High-resolution x-ray photoemission spectrum of the valence bands of gold. *Physical Review B* **1972**, 5 (12), 4709-4714.
- (39) Miao, H.; Ratnasingam, S.; San Pu, C.; Desai, M. M.; Sze, C. C. Dual fluorescence system for flow cytometric analysis of *Escherichia coli* transcriptional response in multi-species context. *Journal of microbiological methods* **2009**, 76 (2), 109-119.
- (40) Vidal, O.; Longin, R.; Prigent-Combaret, C.; Dorel, C.; Hooreman, M.; Lejeune, P. Isolation of an *Escherichia coli* K-12 mutant strain able to form biofilms on inert surfaces: involvement of a new ompR allele that increases curli expression. *Journal of bacteriology* **1998**, 180 (9), 2442-2449.
- (41) Junker, L. M.; Toba, F. A.; Hay, A. G. Transcription in *Escherichia coli* PHL628 biofilms. *FEMS microbiology letters* **2007**, 268 (2), 237-43, DOI: 10.1111/j.1574-6968.2006.00585.x.
- (42) Schaule, G.; Flemming, H.; Ridgway, H. Use of 5-cyano-2, 3-ditolyl tetrazolium chloride for quantifying planktonic and sessile respiring bacteria in drinking water. *Applied and Environmental Microbiology* **1993**, 59 (11), 3850-3857.
- (43) LeChevallier, M. W.; Seidler, R. J.; Evans, T. Enumeration and characterization of standard plate count bacteria in chlorinated and raw water supplies. *Applied and Environmental Microbiology* **1980**, 40 (5), 922-930.
- (44) Scherrer, B. Biostatistique, vol. 1. *Gaëtan Morin éditeur (816 pp.)* **2007**.

- 
- (45) Li, B.; Logan, B. E. Bacterial adhesion to glass and metal-oxide surfaces. *Colloids and surfaces. B, Biointerfaces* **2004**, *36* (2), 81-90, DOI: 10.1016/j.colsurfb.2004.05.006.
- (46) Suttiponparnit, K.; Jiang, J.; Sahu, M.; Suvachittanont, S.; Charinpanitkul, T.; Biswas, P. Role of surface area, primary particle size, and crystal phase on titanium dioxide nanoparticle dispersion properties. *Nanoscale Res Lett* **2011**, *6* (1), 27.
- (47) Maira, A. J.; Yeung, K. L.; Lee, C. Y.; Yue, P. L.; Chan, C. K. Size effects in gas-phase photo-oxidation of trichloroethylene using nanometer-sized TiO<sub>2</sub> catalysts. *Journal of Catalysis* **2000**, *192* (1), 185-196, DOI: 10.1006/jcat.2000.2838.
- (48) Anselme, K.; Davidson, P.; Popa, A. M.; Giazzon, M.; Liley, M.; Ploux, L. The interaction of cells and bacteria with surfaces structured at the nanometre scale. *Acta biomaterialia* **2010**, *6* (10), 3824-46, DOI: 10.1016/j.actbio.2010.04.001.
- (49) Tong, T.; Shereef, A.; Wu, J.; Binh, C. T.; Kelly, J. J.; Gaillard, J. F.; Gray, K. A. Effects of material morphology on the phototoxicity of nano-TiO<sub>2</sub> to bacteria. *Environ Sci Technol* **2013**, *47* (21), 12486-95, DOI: 10.1021/es403079h.
- (50) Pryor, W. A. Oxy-radicals and related species: their formation, lifetimes, and reactions. *Annual Review of Physiology* **1986**, *48* (1), 657-667.

- 
- (51) Takeuchi, H.; Gomi, T.; Shishido, M.; Watanabe, H.; Suenobu, N. Neutrophil elastase contributes to extracellular matrix damage induced by chronic low-dose UV irradiation in a hairless mouse photoaging model. *Journal of dermatological science* **2010**, *60* (3), 151-158.
- (52) D'Haese, W.; Glushka, J.; De Rycke, R.; Holsters, M.; Carlson, R. W. Structural characterization of extracellular polysaccharides of *Azorhizobium caulinodans* and importance for nodule initiation on *Sesbania rostrata*. *Molecular microbiology* **2004**, *52* (2), 485-500.
- (53) Costerton, J. W. Introduction to biofilm. *International Journal of Antimicrobial Agents* **1999**, *11* (3-4), 217-221, DOI: 10.1016/s0924-8579(99)00018-7.
- (54) Vollmer, W.; Blanot, D.; de Pedro, M. A. Peptidoglycan structure and architecture. *FEMS microbiology reviews* **2008**, *32* (2), 149-67, DOI: 10.1111/j.1574-6976.2007.00094.x.
- (55) Sunada, K.; Watanabe, T.; Hashimoto, K. Studies on photokilling of bacteria on TiO<sub>2</sub> thin film. *Journal of Photochemistry and Photobiology A: Chemistry* **2003**, *156* (1), 227-233.
- (56) Maness, P. C.; Smolinski, S.; Blake, D. M.; Huang, Z.; Wolfrum, E. J.; Jacoby, M. A. Bactericidal activity of photocatalytic TiO<sub>2</sub> reaction toward an understanding of its killing mechanism. *Applied and Environmental Microbiology* **1999**, *65* (9), 4094-4098.
- (57) Kiwi, J.; Nadtochenko, V. Evidence for the mechanism of photocatalytic degradation of the bacterial wall membrane at the TiO<sub>2</sub> interface by ATR-FTIR and laser kinetic spectroscopy. *Langmuir : the ACS journal of surfaces and colloids* **2005**, *21* (10), 4631-4641.

- 
- (58) Pal, A.; Pehkonen, S. O.; Yu, L. E.; Ray, M. B. Photocatalytic inactivation of Gram-positive and Gram-negative bacteria using fluorescent light. *Journal of Photochemistry and Photobiology A: Chemistry* **2007**, *186* (2-3), 335-341, DOI: 10.1016/j.jphotochem.2006.09.002.
- (59) Kashket, E. R. Bioenergetics of lactic acid bacteria: cytoplasmic pH and osmotolerance. *FEMS microbiology reviews* **1987**, *3* (3), 233-244.
- (60) Ofek, I.; Beachey, E. H.; Jefferson, W.; Campbell, G. L. Cell membrane-binding properties of group-A Streptococcal lipoteichoic acid. *Journal of Experimental Medicine* **1975**, *141* (5), 990-1003, DOI: 10.1084/jem.141.5.990.
- (61) Zeller, T.; Klug, G. Detoxification of hydrogen peroxide and expression of catalase genes in *Rhodobacter*. *Microbiology* **2004**, *150* (10), 3451-3462.
- (62) Groves, M. R.; De Orue Lucana, D. O. Adaptation to oxidative stress by Gram-positive bacteria: the redox sensing system HbpS-SenS-SenR from *Streptomyces reticuli*. *Appl Microbiol Microb Biotechnol* **2010**.
- (63) Hassan, H. M.; Fridovich, I. Enzymatic defenses against the toxicity of oxygen and of streptonigrin in *Escherichia coli*. *Journal of Bacteriology* **1977**, *129* (3), 1574-1583.
- (64) Jacobs, N.; Conti, S. Effect of hemin on the formation of the cytochrome system of anaerobically grown *Staphylococcus epidermidis*. *Journal of bacteriology* **1965**, *89* (3), 675-679.

- 
- (65) Qiu, J.; Li, S.; Gray, E.; Liu, H.; Gu, Q.-F.; Sun, C.; Lai, C.; Zhao, H.; Zhang, S. Hydrogenation synthesis of blue TiO<sub>2</sub> for high-performance lithium-ion batteries. *The Journal of Physical Chemistry C* **2014**, *118* (17), 8824-8830.
- (66) Di Valentin, C.; Pacchioni, G.; Selloni, A. Reduced and n-type doped TiO<sub>2</sub>: nature of Ti<sup>3+</sup> species. *The Journal of Physical Chemistry C* **2009**, *113* (48), 20543-20552.
- (67) Linsebigler, A. L.; Lu, G. Q.; Yates, J. T. Photocatalysis on TiO<sub>2</sub> surfaces: principles, mechanisms, and selected results. *Chemical reviews* **1995**, *95* (3), 735-758, DOI: 10.1021/cr00035a013.
- (68) Singh, B.; Sharma, N. Mechanistic implications of plastic degradation. *Polymer Degradation and Stability* **2008**, *93* (3), 561-584.
- (69) Wang, N.; Feng, J.; Chen, J.; Wang, J.; Yan, W. Adsorption mechanism of phosphate by polyaniline/TiO<sub>2</sub> composite from wastewater. *Chem. Eng. J.* **2017**, *316*, 33-40, DOI: 10.1016/j.cej.2017.01.066.
- (70) Veuillet, M.; Ploux, L.; Roucoules, V.; Courbeyre, Y.; Gaudichet-Maurin, E. Bacterial adhesion driven by mechanical properties of DMAEMA plasma polymer coatings. *22nd International Symposium on Plasma Chemistry; July 5-10, 2015; Antwerp, Belgium* **2015**.

The following graphic will be used for the TOC:

